Department of Construction Sciences
Solid Mechanics

ISRN LUTFD2/TFHF-17/5218-SE(1-61)

Factors affecting the Relative Crease Strength of paperboard

Master's Dissertation by

Oskar Smedman

Supervisors:
Dr Eric Borgqvist, Tetra Pak
Prof. Johan Tryding, Tetra Pak
Prof. Mathias Wallin, Div. of Solid Mechanics

Examiner:
Prof. Matti Ristinmaa, Div. of Solid Mechanics

Printed by Media-Tryck AB, Lund, Sweden
For information, address:
Division of Solid Mechanics, Lund University, Box 118, SE-221 00 Lund, Sweden
Webpage: www.solid.lth.se

Abstract:
Paperboard is frequently used as a base material in packages. There is folding involved in the conversion process, where a package is formed from a paperboard sheet. However, because direct folding causes undesirable effects such as wrinkles, it must first be creased. The creasing procedure consists of intentionally damaging the material, creating an indentation on the piece, after which the material may be folded as desired.

Constitutive models for paperboard require a large number of parameters to precisely reflect the material behaviour during strongly nonlinear processes such as creasing and folding. In order to increase understanding of the connection between the parameters and the material's behaviour, a parameter study has been conducted and documented in this thesis. Simulation of the procedure is performed in Abaqus/ Standard with the help of its scripting tools. Specifically, the tendency of the material to fold along the crease lines will be measured using the relative crease strength (RCS): the force required to fold a piece of paperboard is considered, and the ratio between the force for a creased and an uncreased package defines the RCS.

Besides the primary goal of studying the RCS, other output data will be extracted to evaluate the material parameters' influence on other responses, as well as the material model itself. Correlations between different responses will also be sought for.

The statistical tool iSight will determine the parameter configurations in each run in order to maximise the amount of information gained from a given number of simulation runs for efficiency; the entire parameter space can not be explored due to the unrealistic amount of time that it would take. When results have been generated, another program, MODDE, statistically analyses the results and determines which factors out of the selected set have a significant effect on the folding procedure.

It is finally concluded that one can get meaningful information by modelling the responses as polynomial functions in terms of the material parameters. It is then discovered that the most important factors are the yield stresses in MD compression and tension, as well as the compressive behaviour in ZD.

Keywords: paperboard, paper mechanics, creasing, solid mechanics, design of experiments, simulation.

Forewords

It all started on a chilly January afternoon. I have conducted my work on Tetra Pak in Lund with indispensable guidance from my terrific supervisors, Dr Eric Borgqvist and Prof. Johan Tryding. I thank Prof. Mathias Wallin very much for introducing me to his neighbour Prof. Tryding in the first place, as well as for his general support throughout this challenging but interesting project, which has given me experience and nurtured my creativity, patience, knowledge and problem solving skills.

Contents

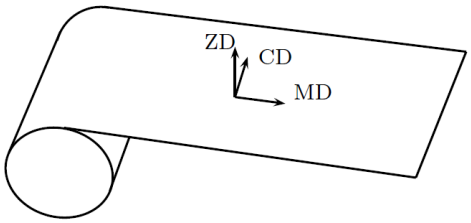

Figure 1.1: Definition of the material directions. [4, p. 2]

1 Background

The mechanical properties of paperboard stem from the production process. A mixture consisting of 0.2–1.0% wood pulp [6, p. 40] and water is transported in the papermaking machine. A nozzle sprays the pulp on a moving web, giving a tendency for the fibres to align in a certain direction because of the differing velocities between the web and the sprayed fibres.

Because of the fibre alignment, the paperboard exhibits its strongest behaviour in this direction, the *machine direction* (MD). The direction perpendicular to MD in the paper's plane is called the *cross direction* (CD). The direction perpendicular to both is the *Z direction* (ZD), see fig. 1.1.

Paperboard, which is a widely used base for packaging, is a material with highly anisotropic mechanical properties. Modelling it with adequate accuracy requires a physically motivated description. This leads to a material model with numerous material parameters, all needed to predict the material response for general geometries, subject to different loads and boundary conditions. Specifically, the focus will lie on the creasing and folding processes, fundamental parts in the package forming process.

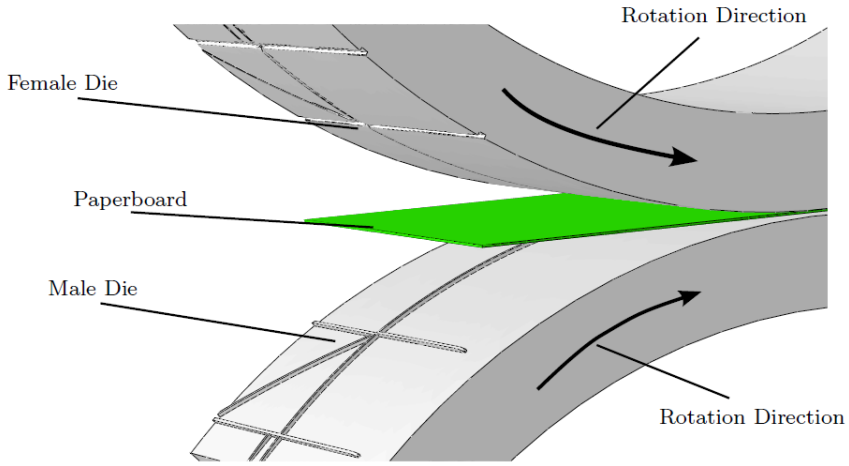

Figure 1.2: Simulation of a rotation creasing machine. [4, p. 8]

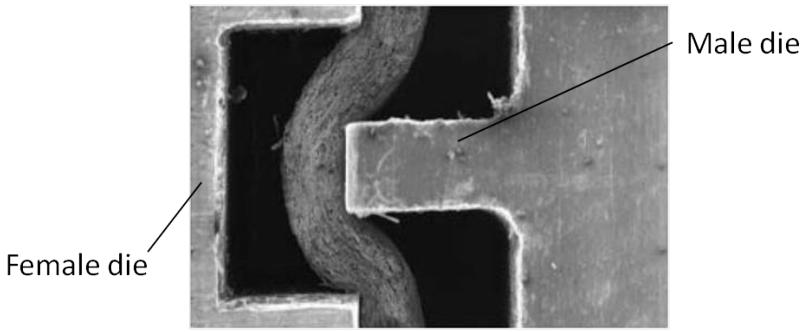

Figure 1.3: Close-up of paperboard being creased.

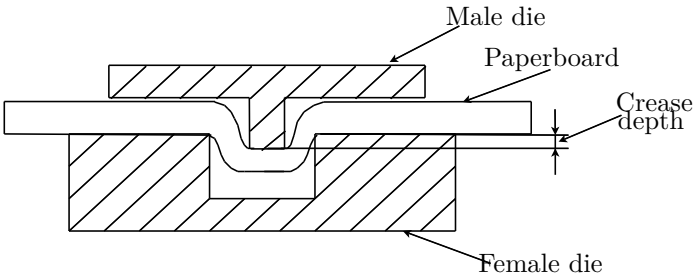

Figure 1.4: Schematic sketch of a creasing tool's cross section.

Paperboard is stored as a roll after production, and in the subsequent converting process it is fed to a rotation creasing machine, see fig. 1.2 for an illustration. To isolate the effects of the creasing itself, a smaller setup is frequently used in experiments, and it will also be applied in this project: the male die is lowered onto the female die, so that an indentation is created in the paperboard, a process known as creasing.

Creasing using this setup is called line creasing. Fig. 1.3 shows a photo of the process, and it is sketched in fig. 1.4. Note that nomenclature is not standardised; in similar tool setups, the male die is sometimes called the 'punch' and the female die simply 'die'.

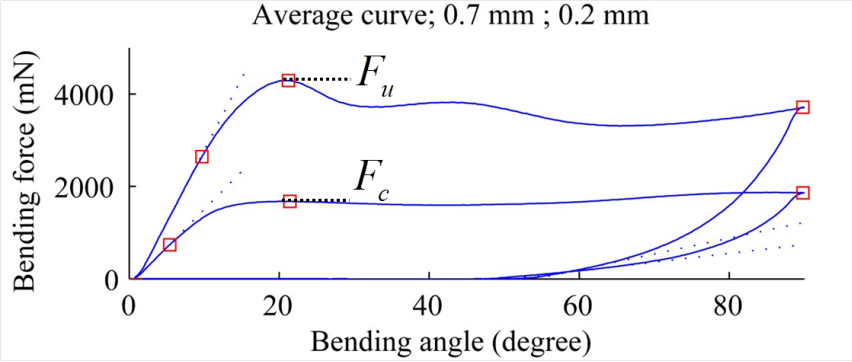

Figure 1.5: Force curves during folding for an uncreased (top) and creased sample (bottom). The maximum force for an uncreased and creased sample are marked with F_u and F_c, respectively.

After the creasing, the paperboard may be folded. Folding after creasing may cause the fibre layers to detach, a phenomenon known as delamination, and the overall effect is that the paperboard folds along the creased line; folding without creasing before is likely to cause undesired effects such as wrinkles, cracks and an uneven scored line. The folding setup is pictured in fig. 1.6.

As a measure of how well the package folds along the creased lines, the industry frequently uses the *relative crease strength* (RCS). The RCS for a material is obtained by measuring the force when folding

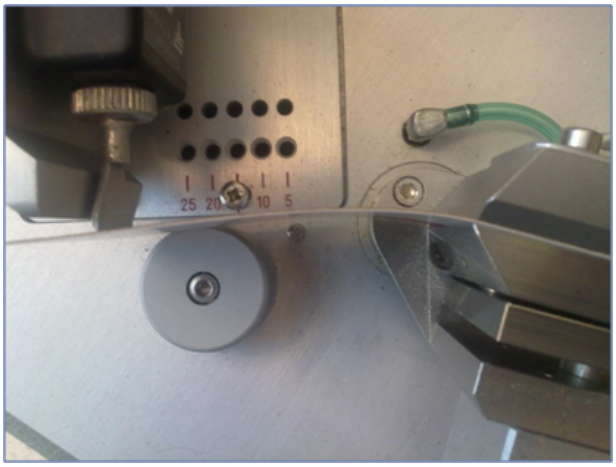

Figure 1.6: Folding setup. The clamps on the right side are lowered to fold the sample.

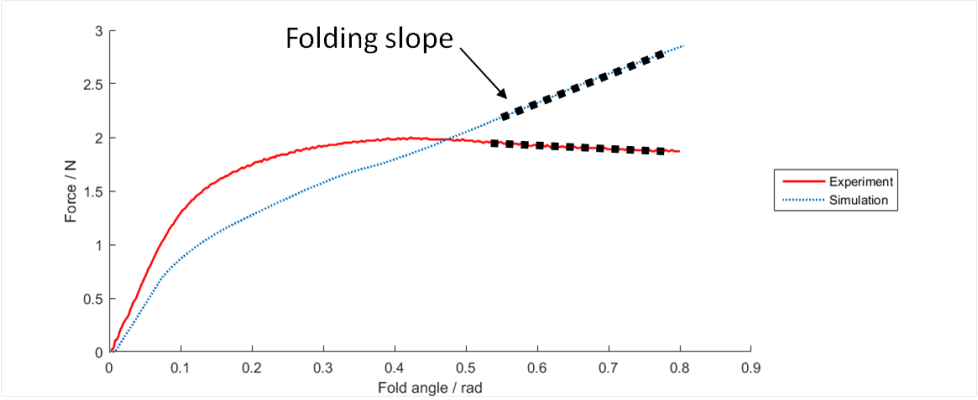

Figure 1.7: Comparison of simulated (blue) and experimental data (red) demonstrating a deviation in stiffness, marked with a dashed line.

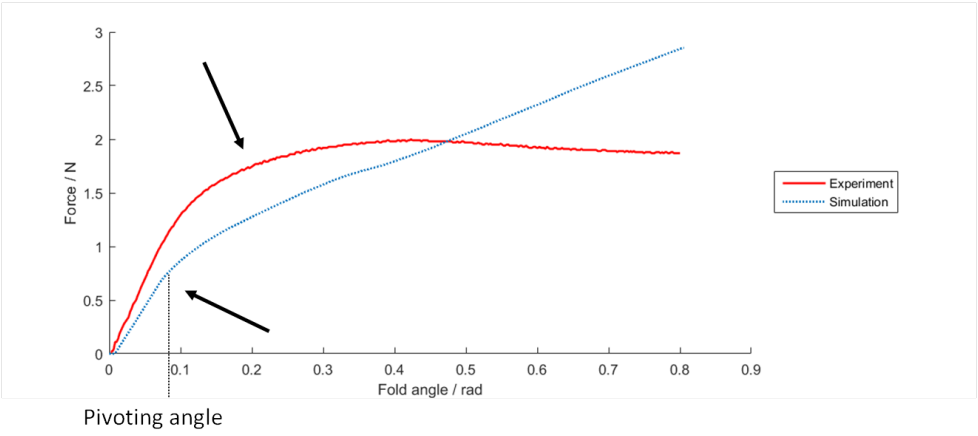

Figure 1.8: Comparison of simulated (blue) and experimental data (red) demonstrating a deviation in where the curve plateaus, marked with arrows. This will later be quantified in terms of the *pivoting angle*.

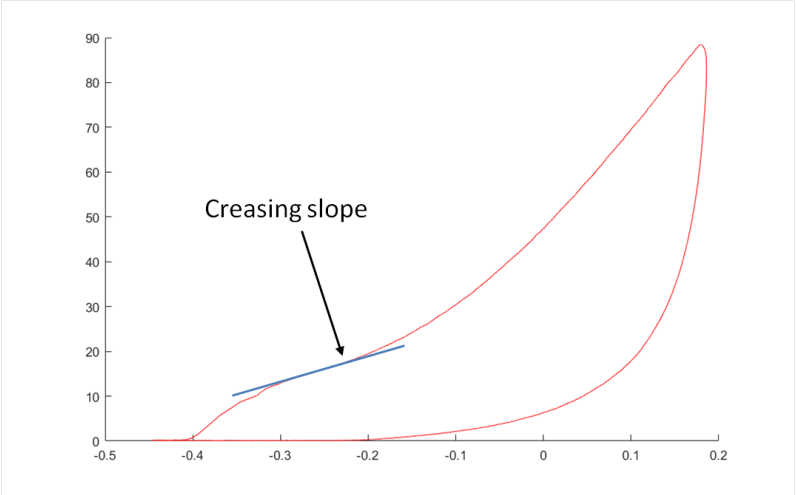

Figure 1.9: Typical force–displacement curve during creasing, obtained using a similar method as in [4, p. 9]. The minimum slope, marked with a blue line, will be examined.

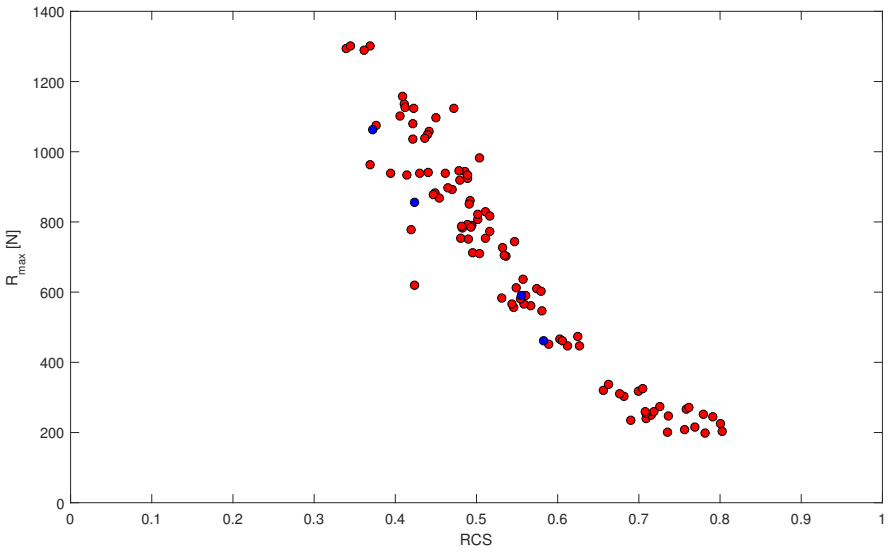

Figure 1.10: Scatter plot of RCS and maximum creasing force. Experimental data using paperboard from different suppliers and varying creasing depths and male die widths in red. Simulations using a fixed material but varying creasing depths and male die widths in blue.

a sample, for one creased sample and one uncreased. The RCS is the maximum force occurring before having folded to 30° for the creased sample, divided by that of the uncreased, cf fig. 1.5. The connection between RCS and foldability can be thought of intuitively: if less energy is used to fold the package, there will be less energy for forming cracks and wrinkles.

In experiments, the force remains roughly constant during folding after a certain point. The simulations do not capture this behaviour, instead predicting the force to increase monotonically, see fig. 1.7. Because of this, the maximum force in the simulations becomes somewhat arbitrary, depending on how far one chooses to fold. The measurement is then restricted to the maximum force occurring before a predetermined folding angle is reached.

In addition to the force during folding, other output data will be gathered to evaluate the model:

- During folding, the slope after the initial phase will be gathered. This is relevant because the material model often overestimates the slope of the folding angle-to-force curve when compared to industrial tests, see fig. 1.7. This is denoted the *folding slope*.
- Likewise, the curve starts levelling off at different points when comparing the simulated curves with those from industrial tests, see fig. 1.8. This will be quantified by measuring the curvature of the force–angle curves. The angle during folding that maximises the curvature will be known as the *pivoting angle*.
- During creasing, the minimum slope of the force–displacement curve is observed to occur when the out-of-plane shear yield stress is reached. [4, p. 8]. This will be denoted the *creasing slope*. See fig. 1.9.
- The maximal force on the male die during creasing has been discovered to be strongly correlated with the RCS when testing paperboard from different suppliers, in combination with different creasing depths and male die widths, see fig 1.10. The relationship will be further investigated here, in terms of material parameters.

All of the data in this section, on which the choice of output responses is based, have been produced prior by Tetra Pak. The data obtained from simulations have been retrieved using a similar procedure as described in section 2.1.2, using a reference material.

Aside from examining individual responses, two models for the RCS will be investigated. The usual strategy for screening is to employ a polynomial regression model. However, because RCS is defined as the *ratio* between two other quantities, polynomial models for each of these quantities are also considered in order to model the RCS indirectly.

In summary, the subject of this thesis is primarily motivated by the desire to understand how an important characteristic such as the RCS is influenced by the numerous material parameters involved in the model. Secondarily, it will offer some insight in how well different aspects in the processes are predicted by the modelling, also giving some suggestions on which aspects in the model to develop in order to improve it.

2 Theory

This section will cover the different theoretical areas used in the work, from mechanics to statistics.

2.1 Model

2.1.1 Summary of material model

The material model for paperboard used in this work was developed in [4] and will be summarised here. Paperboard is an orthotropic material, meaning that one can identify three orthogonal directions in the material that bear a particular property.

For quantities relating to material directions, "1" will stand for MD, "2" will stand for CD, and "3" will finally stand for ZD. Using Voigt notation, the notation will be simplified for the Young's moduli, with E_1 instead of E_{11} and so on. A set of vectors will be defined for reference purposes. A set of unit vectors are defined in the undeformed configuration:

- $\boldsymbol{v}_0^{(1)}$ is aligned with MD,
- $\boldsymbol{v}_0^{(2)}$ is aligned with CD,
- $\boldsymbol{n}_0^{(3)} = \boldsymbol{v}_0^{(1)} \times \boldsymbol{v}_0^{(2)}$ is aligned with ZD.

Let $\boldsymbol{F}$ denote the deformation gradient. It is multiplicatively split into an elastic and a plastic part like $\boldsymbol{F} = \boldsymbol{F}^e\boldsymbol{F}^p$. Let $J^e = \det(\boldsymbol{F}^e)$. In the deformed configuration, then,

- $\boldsymbol{v}^{(1)} = \boldsymbol{F}^e\boldsymbol{v}_0^{(1)}$ is aligned with MD,
- $\boldsymbol{v}^{(2)} = \boldsymbol{F}^e\boldsymbol{v}_0^{(2)}$ is aligned with CD,
- $\boldsymbol{n}^{(3)} = \boldsymbol{v}^{(1)} \times \boldsymbol{v}^{(2)} = J^e\boldsymbol{F}^{e-T}\boldsymbol{n}_0^{(3)}$ is aligned with ZD.

Note that $\boldsymbol{n}^{(3)}$ is defined so that it will always be orthogonal to the other two director vectors. This reflects the layered structure of paperboard, and makes it easier to describe the out-of-plane properties, which must be isolated in order not to be overshadowed by the much-stronger in-plane properties.

Elasticity. The material's behaviour during reversible deformations will be outlined here. It is described in terms of a number of invariants, i.e. quantities that are independent of the global coordinate system. The response during elastic loading is dictated by the specific energy, postulated as a function of these invariants in [4]. First, define the *structural tensors*

$$\boldsymbol{m}^{(p)} = \boldsymbol{v}^{(p)} \otimes \boldsymbol{v}^{(p)}, \quad p \in \{1, 2\}, \tag{2.1}$$

$$\boldsymbol{m}^{(3)} = \boldsymbol{n}^{(3)} \otimes \boldsymbol{n}^{(3)}. \tag{2.2}$$

Let : denote the *double scalar product*, which reduces two tensors to a scalar, defined as $\boldsymbol{A} : \boldsymbol{B} = \operatorname{tr}\left(\boldsymbol{A}^T\boldsymbol{B}\right)$. The invariants are defined as

$$I_{11} = \sqrt{\boldsymbol{m}^{(1)} : \boldsymbol{I}} = \|\boldsymbol{v}^{(1)}\|, \quad I_{12} = \sqrt{\boldsymbol{m}^{(2)} : \boldsymbol{I}} = \|\boldsymbol{v}^{(2)}\|, \tag{2.3}$$

$$I_{23} = \sqrt{\boldsymbol{m}^{(3)} : \boldsymbol{I}} = \|\boldsymbol{n}^{(3)}\|, \quad I_{13} = \sqrt{\boldsymbol{m}^{(3)} : (\boldsymbol{b}^e\boldsymbol{b}^e)}/J^e, \quad J^e = \sqrt{\det(\boldsymbol{b}^e)} = \det(\boldsymbol{F}^e), \tag{2.4}$$

where $\boldsymbol{b}^e = \boldsymbol{F}^e\boldsymbol{F}^{eT}$, the left Cauchy–Green tensor, and $\|\cdot\|$ is the Euclidean norm.

The Kirchhoff stress $\boldsymbol{\tau}$, defined as the product of the true stress and $\det(\boldsymbol{F})$, will be used as a stress measure. The stress–strain relationship is given by the nonlinear constitutive relation

$$\boldsymbol{\tau} = \sum_{i=1}^{3} P_i\boldsymbol{m}^{(i)} + P_4\boldsymbol{I} + \frac{P_5}{J^{e\,2}}\boldsymbol{b}^e\boldsymbol{m}^{(3)}\boldsymbol{b}^e, \tag{2.5}$$

where

$$
\begin{aligned}
P_1 &= \frac{1}{I_{11}}\left(A_1 + A_5 + A_6 + A_4\left(\frac{1}{I_{11}} + \frac{1}{I_{12}}\right)\right) - \frac{1}{{I_{11}}^3}\left(A_1 + A_4(I_{11} + I_{12})\right) \\
P_2 &= \frac{1}{I_{12}}\left(A_2 + A_5 + A_6 + A_4\left(\frac{1}{I_{11}} + \frac{1}{I_{12}}\right)\right) - \frac{1}{{I_{12}}^3}\left(A_2 + A_4(I_{11} + I_{12})\right) \\
P_3 &= \frac{A_5}{{I_{23}}^3} \\
P_4 &= -\frac{A_5}{I_{23}} - A_6 J^e \\
P_5 &= \frac{A_6}{I_{13}} + H^+ A_3\left(\frac{1}{I_{13}} - \frac{1}{{I_{13}}^3}\right) + 2H^- A_7\left(1 - e^{-A_8\left({I_{13}}^2 - 1\right)}\right),
\end{aligned}
\tag{2.6}
$$

where A_i are material constants controlling the elastic behaviour, with two switch functions controlling the behaviour in ZD, which is not symmetric between tension and compression:

$$
\begin{aligned}
H^+ &= \begin{cases} 1 & \text{if } I_{13} - 1 \geq 0 \\ 0 & \text{otherwise,} \end{cases} \\
H^- &= 1 - H^+.
\end{aligned}
\tag{2.7}
$$

A nonlinear relation such as the one described here is crucial for predicting the material response for arbitrary deformations. One might get the impression that the plastic properties are much more important than the elastic, but a simple linearly elastic law will not suffice for the purposes of this work. For example, in compression, the material's stiffness is expected to increase as it is compressed; using a linearly elastic model for large deformations would allow the material to be flattened completely or even turned inside-out using a finite amount of energy. The material model used is consistent with these laws, provided that the A_i are positive. [4, Paper C, p. 9]

The model does not account for damage effects, i.e. degradation of the elastic properties after sufficiently large loads.

Plasticity. For large enough loads, the material will develop irreversible deformations. To determine whether applied stress causes elastic or plastic deformation, a yield function f is introduced, which for any stress $\boldsymbol{\tau}$ satisfies

$$
\begin{aligned}
f(\boldsymbol{\tau}) < 0 \quad &\Leftrightarrow \quad \text{elasticity,} \\
f(\boldsymbol{\tau}) = 0 \quad &\Leftarrow \quad \text{plasticity.}
\end{aligned}
\tag{2.8}
$$

Note that f is dependent on other factors as well, and generally evolves in connection with plasticity, so that the fundamental property (2.8) always holds. The set of all $\boldsymbol{\tau}$ such that $f(\boldsymbol{\tau}) = 0$ is called the *yield surface*.

Some works have used a special type of elements, interface elements, to reflect the separation of fibre layers, for instance [9]. One problem with that approach is that the delamination then can only occur at predefined locations. Instead, the model used in this work is based on continuum elements only, and the yield function will take a very general form.

The yield function is constructed such that the yield surface is built up by a number of sub-surfaces, essentially independent of each other, each with its own slope and distance from the origin in the stress space, and the intersection of these sub-surfaces form a hyper-polyhedron. If hardening occurs in connection with plasticity, these sub-surfaces may be translated independently of each other, giving the model a more general capacity. Because of anisotropy, stress space is six-dimensional, reflecting the six independent components of the stress tensor. For every component, there is one sub-surface delimiting in the positive direction and one in the negative, i.e. 12 sub-surfaces in total.

Each sub-surface is defined by a normal direction together with the distance from the origin. The normal direction tensors are defined as

$$
\boldsymbol{n}_s^{(\nu)} = \sum_{i=1}^{3}\sum_{j=1}^{3} N_{ij}^{(\nu)} \bar{\boldsymbol{v}}^{(i)} \otimes \bar{\boldsymbol{v}}^{(j)},
\tag{2.9}
$$

which are expressed in the normed director vectors

$$\bar{\boldsymbol{v}}^{(p)} = \frac{\boldsymbol{v}^{(p)}}{\left\|\boldsymbol{v}^{(p)}\right\|}, \quad p \in \{1, 2\} \tag{2.10}$$

$$\bar{\boldsymbol{v}}^{(3)} = \frac{\boldsymbol{n}^{(3)}}{\left\|\boldsymbol{n}^{(3)}\right\|}, \tag{2.11}$$

and $N_{ij}^{(\nu)}$ are constants, which all remain constant irrespective of the material, with a few exceptions: $N_{ij}^{(1)}, N_{ij}^{(2)}$ are determined by the Poisson's ratios ν_{12}, ν_{21} – usually regarded as elastic parameters, the Poisson's ratios directly influence the plastic behaviour. This comes from assuming that the axial–lateral plastic strain rate ratios are equal to that of the total strain [4, Paper A, p. 15], and so ν_{12} (and ν_{21}) appear in the yield surface normals, introducing a coupling between yield stresses and pre-straining, cf fig. 2.4.

Furthermore, $N_{ij}^{(9)}, \ldots, N_{ij}^{(12)}$ are determined by a parameter denoted m. Straining in MD essentially causes the fibres to push against each other, and the out-of-plane shear yield stress increases, as examined in [12], which is why m will be associated with paper–paper friction. See fig. 2.3.

A yield function using this sub-surface approach was originally proposed in [13]. It's constructed by a sum of convex polynomials and appears in [4, p. 16] and will be summarised here. In terms of the Kirchhoff stress tensor $\boldsymbol{\tau}$ and surface normals $\boldsymbol{n}_s^{(\nu)}$ the yield function can be expressed as

$$f(\boldsymbol{\tau}, \tau^{(1)}, \ldots, \tau^{(n)}, \boldsymbol{n}_s^{(1)}, \ldots, \boldsymbol{n}_s^{(n)}) = \sum_{\nu=1}^{n} \chi^{(\nu)} \left(\frac{\boldsymbol{\tau} : \boldsymbol{n}_s^{(\nu)}}{\tau^{(\nu)}} \right)^{2k} - 1, \tag{2.12}$$

where each term in the sum is associated with a simple loading case, see table 2.1; the number of sub-surfaces used is $n = 12$. $\tau^{(\nu)}$ are quantities controlling the distance to each sub-surface from the origin in stress space. They are related (but not necessarily equal) to the yield stresses in simple loading cases. The initial value of $\tau^{(\nu)}$ is denoted $\tau_0^{(\nu)}$, see fig. 2.1. $\tau^{(\nu)}$ evolves when plasticity takes place, and the evolution is represented by the (non-negative) hardening variables $K^{(\nu)}$:

$$\tau^{(\nu)} = \tau_0^{(\nu)} + K^{(\nu)}(\kappa^{(\nu)}). \tag{2.13}$$

The hardening variables $K^{(\nu)}$ are dependent on a set of internal variables $\kappa^{(\nu)}$, which are state variables which denote the amount of plastic straining that has occurred. The internal variables control the hardening in the following way:

$$\begin{aligned} K^{(\nu)} &= a_\nu \ln(b_\nu \kappa^{(\nu)} + 1) \quad \text{for } \nu \in \{1, 2, 3, 6\}, \\ K^{(7)} &= a_7 \kappa^{(7)}. \end{aligned} \tag{2.14}$$

Other hardening variables are zero, resulting in ideal plasticity for these loading cases. Plastic strains develop according to

$$\boldsymbol{L}^p = \boldsymbol{F}^{e-1} \left(\sum_{\gamma=1}^{12} \dot{\lambda} \frac{2k\chi^{(\gamma)}}{\tau^{(\gamma)}} \left(\frac{\boldsymbol{\tau} : \boldsymbol{n}_s^{(\gamma)}}{\tau^{(\gamma)}} \right)^{2k-1} \boldsymbol{n}_s^{(\gamma)} \right) \boldsymbol{F}^e, \tag{2.15}$$

where $\boldsymbol{L}^p$ is the spatial plastic velocity gradient, and $\dot{\lambda}$ is the *plastic multiplier*, controlling the size of plastic strain development. During purely elastic deformation, $\dot{\lambda} = 0$.

The internal variables evolve as

$$\dot{\kappa}^{(\nu)} = \dot{\lambda} \frac{2k\chi^{(\nu)}}{\tau^{(\nu)}} \left(\frac{\boldsymbol{\tau} : \boldsymbol{n}_s^{(\nu)}}{\tau^{(\nu)}} \right)^{2k}. \tag{2.16}$$

The $\chi^{(\nu)}$ in the yield function (2.12) are switch functions, controlling whether specific sub-surfaces are active, defined as

$$\chi^{(\nu)} = \begin{cases} 1 & \text{if } \boldsymbol{\tau} : \boldsymbol{n}_s^{(\nu)} > 0 \\ 0 & \text{otherwise,} \end{cases} \tag{2.17}$$

Table 2.1: Numbering of loading cases.

ν	Loading case
1	MD tension
2	CD tension
3	MD/CD shear (positive)
4	MD compression
5	CD compression
6	MD/CD shear (negative)
7	ZD compression
8	ZD tension
9	MD/ZD shear (positive)
10	MD/ZD shear (negative)
11	CD/ZD shear (positive)
12	CD/ZD shear (negative)

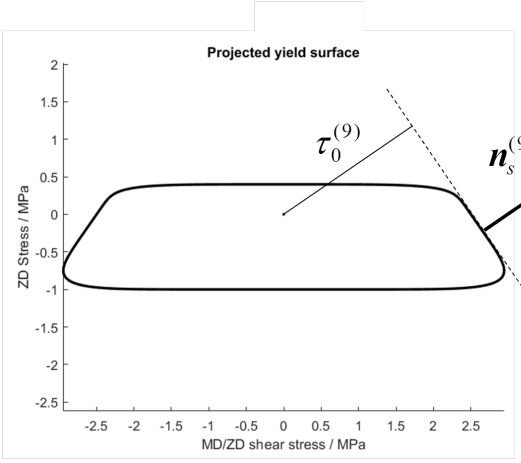

Figure 2.1: Initial yield surface projected onto the (τ_{13}, τ_{33}) plane, illustrating the quantities $\tau_0^{(9)}$ and $\boldsymbol{n}_s^{(9)}$.

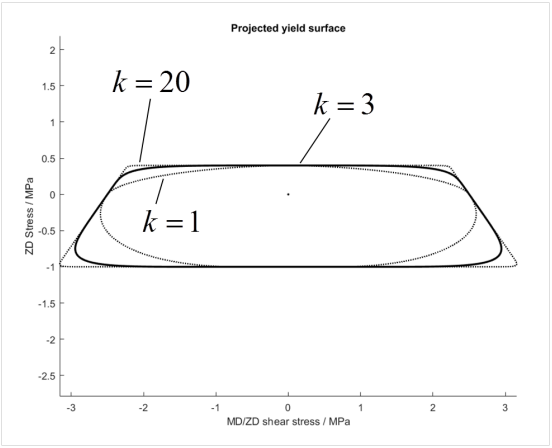

Figure 2.2: Initial yield surface for different k, projected onto the (τ_{13}, τ_{33}) plane.

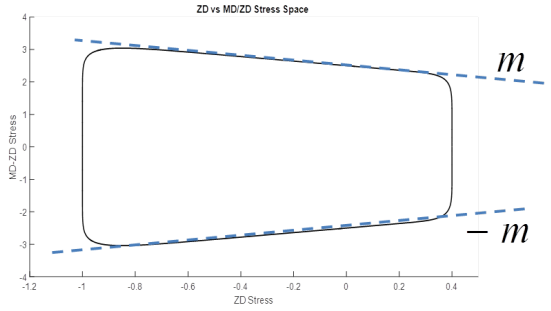

Figure 2.3: Initial yield surface projected onto the (τ_{33}, τ_{13}) plane, illustrating the friction parameter m.

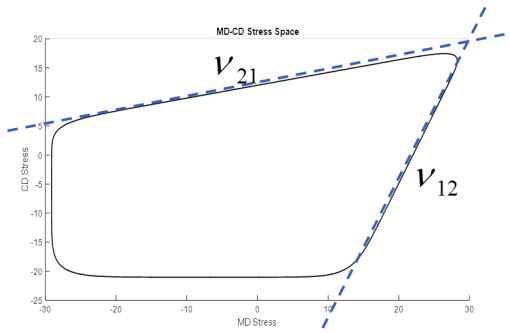

Figure 2.4: Initial yield surface projected onto the (τ_{11}, τ_{22}) plane, illustrating the Poisson's ratios ν_{12}, ν_{21}.

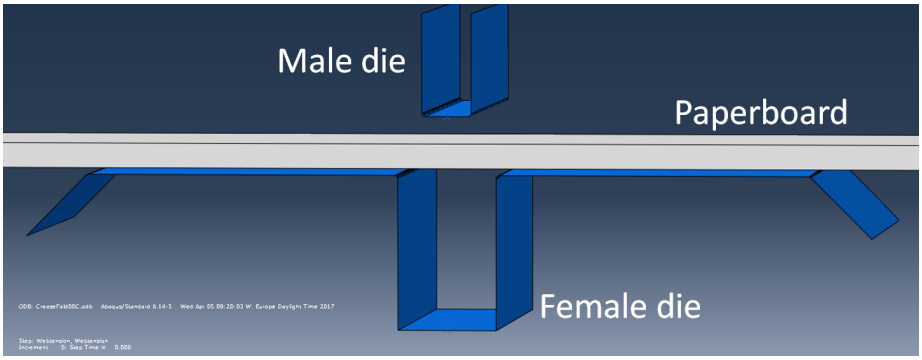

Figure 2.5: Active parts of the model during creasing.

While $\kappa^{(\nu)}$ may be defined for all sub-surfaces ν, they are only essential in the cases where hardening occurs, i.e. for $\nu \in \{1, 2, 3, 6, 7\}$. The consistency condition $f = 0$ is enforced to determine $\dot{\lambda}$, resulting in a complete differential–algebraic system of equations. The positive integer k in (2.12) is associated with smoothing of the sub-surface intersections, see fig. 2.2.

In short, this yield function provides a convex yield surface and is able to model a high degree of anisotropy, as is exhibited by paperboard.

Table 2.2: Summary of model components.

Quantity	Notes
$A_1, \ldots, A_8$	Elastic material constants.
$\tau^{(\nu)}$	Orthogonal distance from yield surface ν to the origin in stress space. ($\nu \in \{1, \ldots, 12\}$)
$\tau_0^{(\nu)}$	Initial value of $\tau^{(\nu)}$.
$K^{(\nu)}$	Hardening variable for sub-surface ν; $\tau^{(\nu)} = \tau_0^{(\nu)} + K^{(\nu)}$.
a_ν, b_ν	Constants controlling the hardening for sub-surface ν. ($\nu \in \{1, 2, 3, 6, 7\}$)
$\kappa^{(\nu)}$	Internal variables, related to plastic strain. ($\nu \in \{1, \ldots, 12\}$)
k	Yield surface exponent, controlling the smoothing of the yield surface near intersections.
$\boldsymbol{n}_s^{(\nu)}$	Tensor representing the normal to sub-surface ν. ($\nu \in \{1, \ldots, 12\}$)
m	Paper friction parameter, controlling the slope of some sub-surfaces.
ν_{12}, ν_{21}	Poisson's ratios, also controlling the slopes of some sub-surfaces.

2.1.2 Creasing–folding model

To simulate the aforementioned experimental setup, in which a piece of paperboard is folded and possibly creased beforehand, the finite element program Abaqus/Standard is used. The paperboard sample is a cuboid measuring $80 \times 3\,\text{mm}$, with a thickness of $0.4\,\text{mm}$, aligned so that MD runs along its length. Relevant information will be gathered from the simulations, namely the force history on the load cell during folding, as well as the force history on the male die during loading. Because dynamical effects are assumed to be negligible, the problem will be considered quasi-static.

Furthermore, the material is modelled as being homogeneous; in reality, paperboard usually consists of multiple layers of paperboard types with differing properties.

Let z be a coordinate along the thickness, with $z = 0$ coinciding with the underside of the paperboard at its initial placement, see fig. 2.7. Let x be a coordinate along MD, with $x = 0$ being the symmetry plane that divides the male and female dies in half, see fig. 2.13. The paperboard then stretches from $x = -41\,\text{mm}$ to $x = 39\,\text{mm}$. The model is shown in figures 2.5–2.6. The test contains the following steps, in chronological order:

- Web tension: the board is strained by displacing the right face by $0.15\,\text{mm}$.

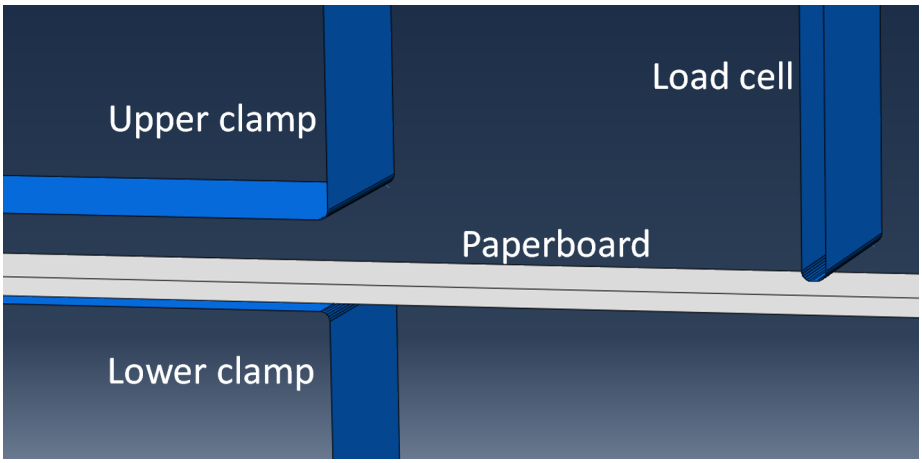

Figure 2.6: Active parts of the model during folding.

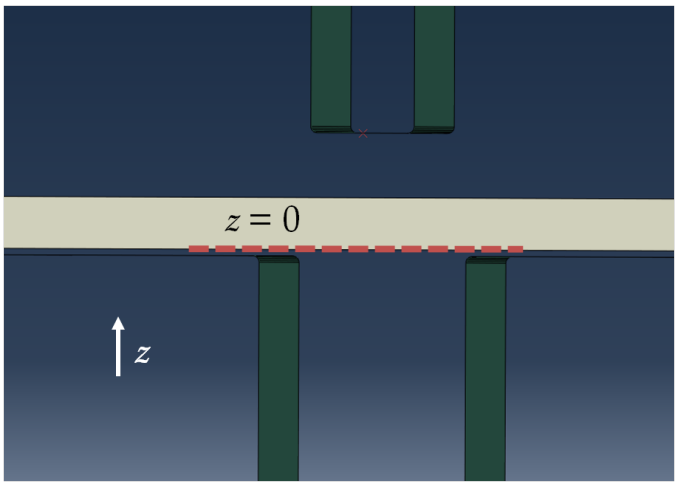

Figure 2.7: Definition of the plane $z = 0$.

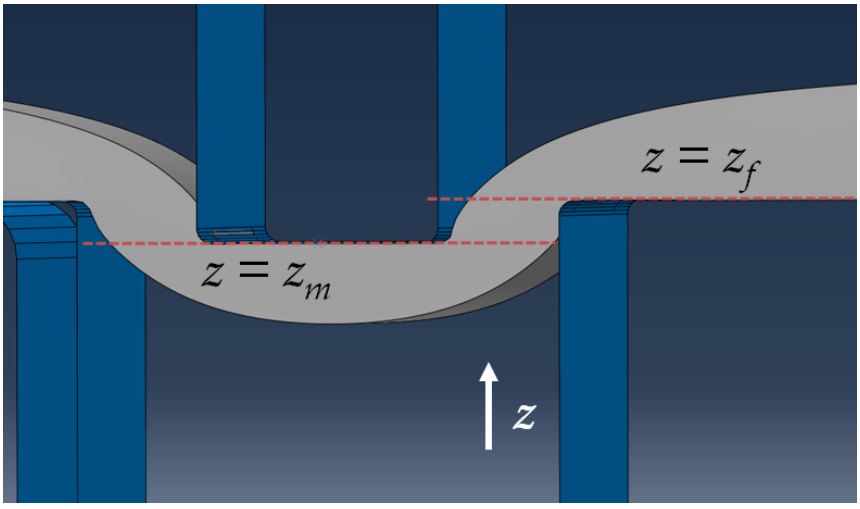

Figure 2.8: Geometry of the dies during creasing: $z_m = -0.15\,\text{mm}$, $z_f = -0.01\,\text{mm}$.

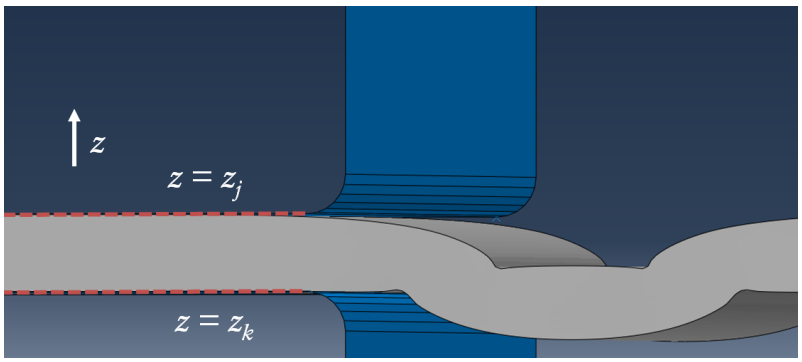

Figure 2.9: Geometry of the clamps before folding: $z_j = 0.3955\,\text{mm}$, $z_k = 0.0045\,\text{mm}$.

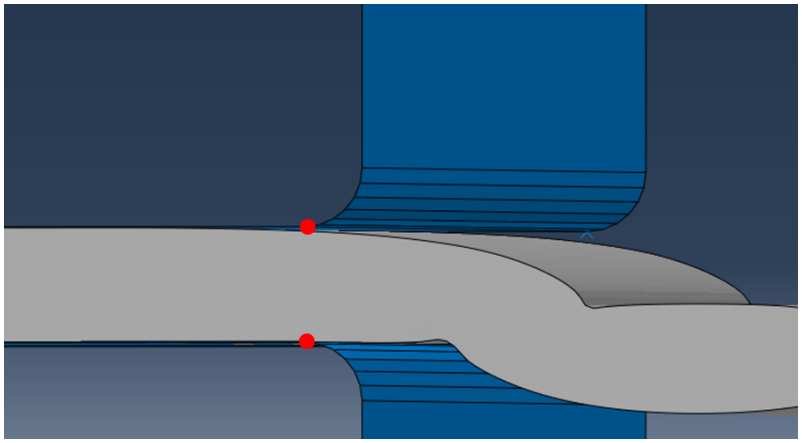

Figure 2.10: Rotation points for the clamps, marked with dots.

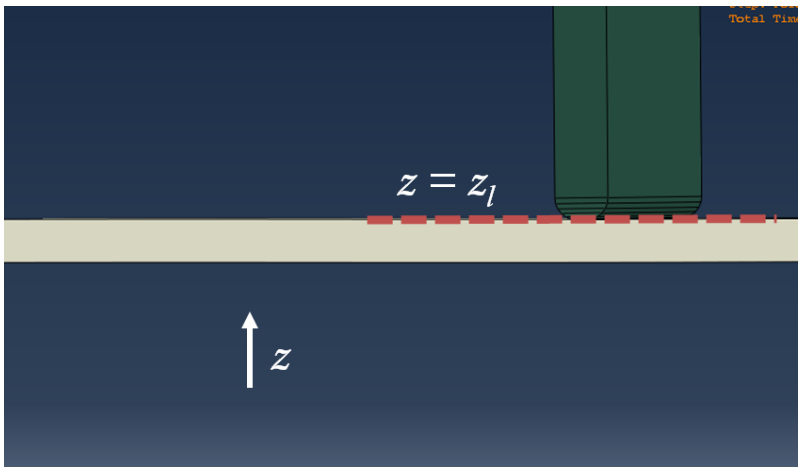

Figure 2.11: Geometry of the load cell during creasing: $z_l = 0.36\,\text{mm}$.

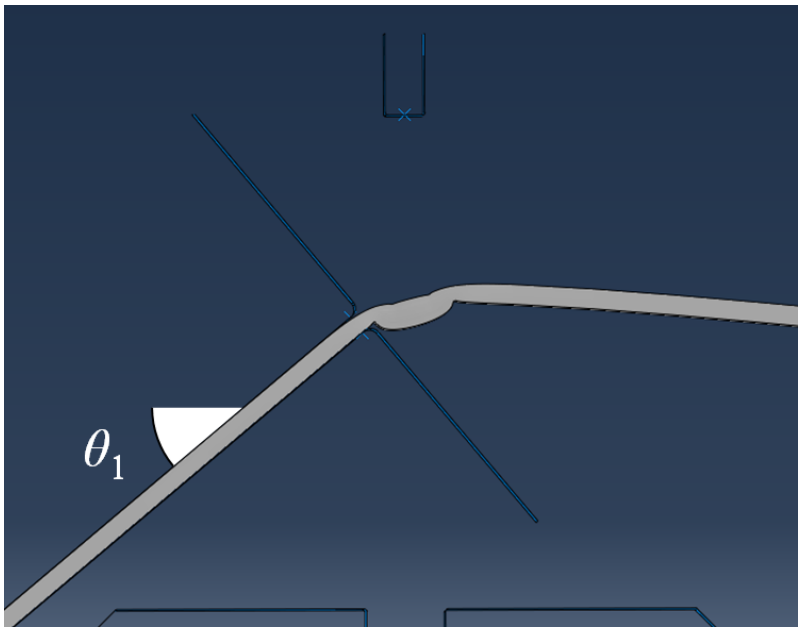

Figure 2.12: Definition of the folding angle θ_1.

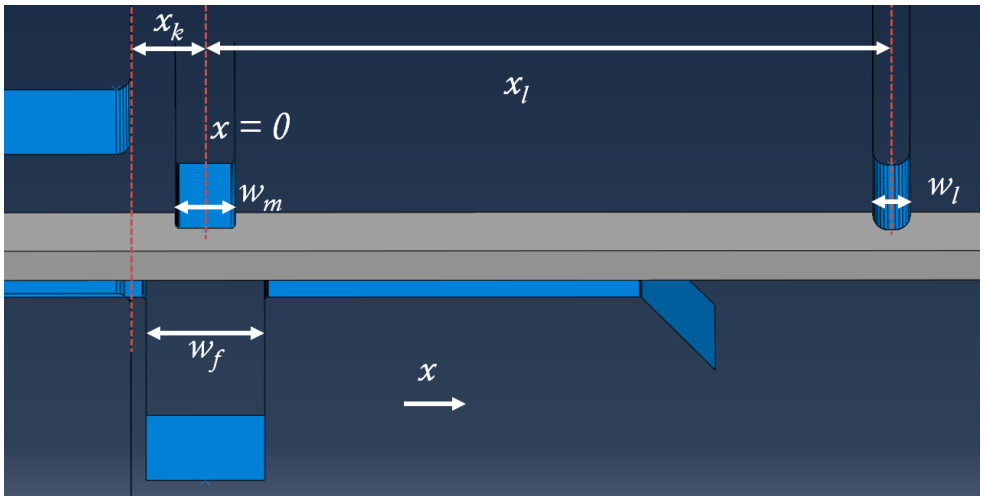

Figure 2.13: Initial dimensions of the model: $w_f = 1.6\,\text{mm}$, $w_m = 0.8\,\text{mm}$, $w_l = 0.5\,\text{mm}$, $x_k = 1\,\text{mm}$, $x_l = 9.25\,\text{mm}$.

- The female die, whose gap width is 1.6 mm, is moved upward until its top plane is located at $z = -0.01$ mm, almost touching the paper. See fig. 2.8.
- Creasing: the male die, with a width of 0.8 mm, is moved downward until the plane of its underside is located at $z = -0.15$ mm. The position of the female die gives a crease depth of 0.14 mm, equal to $z_f - z_m$ according to fig. 2.8. This step is skipped in the uncreased jobs.
- Crease unloading: the male die is moved back.
- The male and female dies are inactivated, while the clamps and the load cell, initially inactive, are now activated. The right face is returned to its original position, removing web tension, while the load cell is lowered such that its lower end is at $z = 0.36$ mm, see fig. 2.11.
- Clamping: the left half of the paperboard is clamped by displacing the clamps until the clamp gap, the distance between them, is 0.391 mm, see fig. 2.9. The distance from the clamps' edges to the center of the dies is 1 mm, see fig. 2.13.
- Folding: keeping this separation, the clamped section is rotated counter-clockwise by an angle of θ_1, see fig. 2.12. The center of rotation for the clamps is the point where the fillet meets the flat section touching the paper, see fig. 2.10. It is folded by contact with the load cell, whose center is positioned at 9.25 mm to the right from that of the paperboard, see fig. 2.13. The cell's with is 0.5 mm.
  - In the beginning of this step, a boundary condition is applied to the top edge of the paperboard's right face constraining the MD component of its position, in order to avoid bifurcations where the solution becomes unphysical. The BC is removed shortly, only after a few degrees of folding, in order not to influence the solution.

The folding angle used is $\theta_1 = 40°$, and the measurements are illustrated in figures 2.8–2.13. All the components of the model except for the paperboard are modelled as rigid bodies. The rigid parts are given rounded corners, or 'fillets', in order to help the contact algorithm in Abaqus [1]. The male and female dies have fillets of radius 0.05 mm, and those of the load cell and measure 0.2 mm.

The paperboard uses 20 continuum elements through the thickness and only one element through CD, since the problem is essentially a plane problem. Through MD, we take advantage of the fact that some regions undergo small deformations, and so some parts are meshed more finely than others. Near the creasing tools and the load cell, 33 elements per mm are used. Outside these critical regions, the density varies from 0.62 mm^{-1} in a vicinity, down to 0.31 mm^{-1} even farther away. In total, the paperboard mesh consists of around 4,000 elements.

2.2 Solution procedure

The quasi-static problem is simulated in Abaqus/Standard. As the problem is nonlinear, loads are always applied in *increments*. The Newton–Raphson method is used to find the equilibrium solution at the next increment. [1]

2.3 Statistics

In order to find the factors which affect RCS the most, some statistical techniques will be used. It is assumed that the response may be expressed as a polynomial depending on the factors, as an approximation. For polynomial regression, there are three major models to choose from:

- Linear: $y = c_0 + c_1x_1 + c_2x_2 + \ldots + E$ (2.18)
- Interaction: $y = c_0 + c_1x_1 + c_2x_2 + c_3x_1x_2 + \ldots + E$ (2.19)
- Quadratic: $y = c_0 + c_1x_1 + c_2x_2 + c_3x_1x_2 + c_4x_1^2 + c_5x_2^2 + \ldots + E$ (2.20)

x_i are the parameters, c_j are the regression coefficients, and E denotes the error, i.e. the deviation from the chosen model. Information about which factors affect the response is obtained by examining the

regression coefficients: if large, it indicates a large influence, while a near-zero coefficient indicates that the effect is insignificant.

Clearly, the number of coefficients increases with the number of variables. For d variables, a linear model contains $1+d$ coefficients, a full interaction model has $1+d(d+1)/2$ coefficients, and a full quadratic model has $1+d(d+3)/2$ coefficients. As the number of coefficients increases, the estimates will in general be less precise for a fix number of simulations.

For the main screening procedure, a linear model is chosen. This does not mean that the behaviour is assumed to be linear – this is only done to capture the main effects that factors have on average, to make it easy to interpret. Later on, if the samples are appropriately chosen, one may consider adding interactional and quadratic terms to establish a predictive model, if the linear one is not sufficient.

We will symbolically let the values range from -1 to 1. After this transformation, the values are said to be *coded*. This way, an entire material setting may be represented by a (row) vector of such coded values. To represent the whole experiment, multiple vectors will be stacked and form the *design matrix*, denoted $\boldsymbol{X}$. For some variable x, if $x \in [x_{min}, x_{max}]$, then it is transformed to its coded value $\bar{x}$ by an affine relationship fulfilling $x = x_{max} \Leftrightarrow \bar{x} = 1$ and $x = x_{min} \Leftrightarrow \bar{x} = -1$. This transformation and its inverse are given by

$$\bar{x} = \frac{2x - x_{min} - x_{max}}{x_{max} - x_{min}} \tag{2.21}$$

$$x = \frac{x_{max}(\bar{x}+1) - x_{min}(\bar{x}-1)}{2}. \tag{2.22}$$

One advantage of using coded values is that it forces all variables to the same order of magnitude. Furthermore, it also removes a linear correlation between x and x^2 for any variable x.

Coding the variables also allows for a simple interpretation of the regression coefficients: if the regression coefficient of parameter x is c, then the response increases with c when x is raised from the average to the maximum – at least in the ideal case where the error E is zero – if all other parameters are kept constant.

A related measure is the *effect*, equal to the double of the regression coefficient. This is instead interpreted as the change in response when a parameter is changed from the minimum to the maximum, if all other parameters are kept constant.

2.3.1 Sampling method

We emphasise that the goal is to gain an understanding on the effects of some elected parameters on the RCS. For this purpose, the aforementioned simulation is executed using materials with different specified properties. The set of all possible parameter combinations is known as *parameter space*. The configuration of points in the parameter space needs to be chosen somehow. Parameter space contains an infinite number of points, and to proceed, it is assumed that every response is a continuous function of the material parameters. Thus, the response can be understood by surveying a finite amount of points.

One may consider the classical one-factor-at-a-time (OFAT) approach, namely to alter one parameter at time while keeping all the others at a fix, nominal value. Although this method is intuitive, it poses a number of problems:

- Results are heavily dependent on the starting point.
- Interaction effects between parameters are not accounted for.
- Effects and noise are confounded.
- It explores a very small subset of the parameter space.

Seemingly, OFAT gives a very limited understanding of the overall effect from any parameter in the design space. Instead, a *design-of-experiments* (DOE) approach is used. In order to make sense of the results to be found, the design points have to be sampled with care. If an effect is observed, is it because one parameter changed, or another one, or a combination of multiple parameters?

In order to be able to separate the parameters' effects from each other, an *orthogonal design* will be used, in which the inputs are essentially uncorrelated. Traditional DOE sampling methods will usually

place all parameters at their extremes, which can be thought of as sampling all the corners in a cube (or hypercube). The further away two points are from each other, the more certainty when measuring the slope. However, because the tests are simulated rather than physical, there is no variability at all; results are entirely deterministic. Any deviation from the regression model comes from the inaccuracy of the regression model itself, rather than noise.

In loose terms, because the response is assumed to be of low variation around any given point, just like any other continuous function, having points near each other is a loss of efficiency. With this in mind, the chosen method will be one that explores as much of the space as possible, a *space-filling design*.

The response is assumed to be nonlinear, and with no other information available in advance, there is no way to predict the response for an arbitrary set of material parameters. For this reason, a space-filling design is desirable. Furthermore, if only the extremes were to be measured, the results would be too heavily influenced by the parameters' behaviour in the extremes, if the nonlinearity assumption turns out to be correct; the average behaviour that each parameter exhibits is more interesting.

The method finally chosen is *optimal Latin hypercube sampling*, with which points will be sampled evenly throughout parameter space. Optimal Latin hypercube sampling is a special case of *Latin hypercube sampling*. If n tests are planned, each parameter range will be divided in n intervals. For each trial, every parameter will be assigned a random value in a different interval, so that each interval is used only once. The optimal Latin hypercube processes the original design chosen, optimising it so that the minimum distance between any two points is maximised, ensuring that no two points are close too each other.

The initially generated design matrix is referred to as the *trial design matrix*, $\boldsymbol{X}_0$. The trial design matrix used can be seen in section A.2. In this case, a true Latin hypercube may not be used, since one parameter (later introduced as k) only takes discrete values, the set of which is much smaller than the number of tests, i.e. some of the n intervals will contain multiple values. After generating the matrix, it will be updated to reflect the allowed values of k.

It might occur that more sample points are desired than what has been generated in the design. To add more points, a new Latin hypercube will be generated, with a redundant amount of points. All points that are sufficiently far away from the points already used are then added to complete the design. The result will most likely not qualify as a Latin hypercube, but will be good enough since the new points are forced to be sufficiently far away from the old points.

2.3.2 Fitting

A statistical model will be fitted to match the results using polynomial regression. (2.18) may be written in matrix form as

$$\boldsymbol{y} = \boldsymbol{X}\boldsymbol{c} + \boldsymbol{E}, \tag{2.23}$$

where $\boldsymbol{y}$ is a vector of sampled responses, $\boldsymbol{X}$ is the design matrix, $\boldsymbol{c}$ is the vector of coefficients, and $\boldsymbol{E}$ is the error vector. To attain an optimal fit, the error must be minimised. Rearrangement gives $\boldsymbol{E} = \boldsymbol{y} - \boldsymbol{X}\boldsymbol{c}$. Define the argmin function which returns the argument that minimises a given quantity, assuming that one such value exists:

$$f(\boldsymbol{x}^*) = \min_{\boldsymbol{x}\in S} f(\boldsymbol{x}) \quad \Leftrightarrow \quad \boldsymbol{x}^* = \operatorname*{argmin}_{\boldsymbol{x}\in S} f(\boldsymbol{x}). \tag{2.24}$$

Another function, argmax, is defined analogously. To find the coefficient set $\boldsymbol{c}^*$ that minimises the error by least-squares fitting, we get

$$\boldsymbol{c}^* = \operatorname*{argmin}_{\boldsymbol{c}\in\mathbb{R}^m} \left\|\boldsymbol{y} - \boldsymbol{X}\boldsymbol{c}\right\|^2, \tag{2.25}$$

where m is the number of coefficients, i.e. the size of the coefficient vector. It turns out that if $\boldsymbol{X}$ has full rank, the solution is found through the matrix multiplication

$$\boldsymbol{c}^* = \left(\boldsymbol{X}^T\boldsymbol{X}\right)^{-1}\boldsymbol{X}^T\boldsymbol{y}. \tag{2.26}$$

which solves the so-called normal equations. There are multiple ways to arrive at this result; MODDE does not use this, instead opting for singular value decomposition. For some variable set $\boldsymbol{x}$, the predicted response $\hat{y}(\boldsymbol{x})$ is then given by

$$\hat{y} = \boldsymbol{x}\boldsymbol{c}^*. \tag{2.27}$$

The quadratic model will be fitted iteratively, excluding terms with very low significance and re-fitting to maximise its ability to predict, quantified by Q^2. This measure is defined in the following section.

2.3.3 Model evaluation

After having fitted the regression model to the results, it needs to be analyzed. Assume that n tests are used. Let y_i and $\bar{y}$ denote the response of test i and the average of the responses, respectively, so that

$$\bar{y} = \frac{1}{n}\sum_{i=1}^{n} y_i. \tag{2.28}$$

Let $\hat{y}_i$ denote the predicted response of test i according to (2.27). To quantify the predictive ability of a model, first define the deletion operator $\boldsymbol{J}_i : \mathbb{R}^{n\times m} \to \mathbb{R}^{(n-1)\times m}$, which removes row i from a matrix or column vector. Also let y_i' be the predicted response of test i for a regression model constructed by excluding test i, so that the coefficient set $\boldsymbol{c}_i'$ satisfies

$$\boldsymbol{c}_i' = \underset{\boldsymbol{c}_i'\in\mathbb{R}^m}{\operatorname{argmin}} \left\|\boldsymbol{J}_i\boldsymbol{y} - \boldsymbol{J}_i\boldsymbol{X}\boldsymbol{c}_i'\right\|^2, \tag{2.29}$$

from (2.27) giving

$$y_i' = \boldsymbol{x}_i\boldsymbol{c}_i', \tag{2.30}$$

if $\boldsymbol{x}_i$ is the ith row of the design matrix $\boldsymbol{X}$. The *sum of squares* (SS) is defined as

$$S_S = \sum_{i=1}^{n} (y_i - \bar{y})^2. \tag{2.31}$$

The *residual sum of squares* (RSS) is defined as

$$S_{RS} = \sum_{i=1}^{n} (y_i - \hat{y}_i)^2. \tag{2.32}$$

The *predicted residual error sum of squares* (PRESS) is defined as

$$S_{PRES} = \sum_{i=1}^{n} (y_i - y_i')^2. \tag{2.33}$$

From these error measures, we define

$$R^2 = 1 - \frac{S_{RS}}{S_S}, \tag{2.34}$$

$$Q^2 = 1 - \frac{S_{PRES}}{S_S}. \tag{2.35}$$

R^2 is the *coefficient of determination*, which measures how well the model fits the data, by comparing it to the predicted responses. The Q^2 statistic, which lacks a standardised name, measures how well it predicts unknown data, by comparing every measured response to how well all the other responses predict it. Both of these values are 1 in an ideal case. However, because R^2 can be increased by arbitrarily including more terms, without necessarily improving the validity of the model, Q^2 is more interesting. In rough terms, a model may be considered to be good if $Q^2 \gtrsim 0.5$ and $R^2 - Q^2 \lesssim 0.3$. [5, p. 78]

Every estimated coefficient will have an associated *confidence interval*, which will be used to classify them by significance. Let c be the estimate of a regression coefficient, and its 95% confidence interval $[c-\Delta, c+\Delta]$. Δ is known as the *margin of error*. The true value of the regression coefficient is unknown; the confidence interval most likely contains the true value. Specifically, the confidence interval includes all c^* such that the probability of measuring c or a larger deviation if the true value is c^* is larger than 5%.

If the confidence interval contains zero, one can not rule out the possiblity that a variable has no effect on the response. The coefficients will be classified in three categories, depending on significance:

- Insignificant if $\Delta > c$, meaning that the confidence interval contains zero.
- Significant if $\Delta \leq c < 3\Delta$. The possibility that the coefficient is zero may certainly be ruled out, but the exact value can not be stated reliably.
- Very significant if $c \geq 3\Delta$. If the confidence interval is rather small relative to the parameter, its value is almost certain.

This classification will give an overview of how the response is affected by the factors.

2.3.4 Summary of statistics section

- A large number of parameter configurations are sampled to fill out parameter space.
- Responses are calculated for these configurations.
- A polynomial is fitted to the response, as a function of the material parameters.
  - If using a linear polynomial, its coefficients may be interpreted as the average effect from every individual parameter.
  - This polynomial may potentially be used to predict new values, if the fit is sufficiently good.

3 Methodology

The material model contains numerous parameters, so the scope must be constrained by electing a number of parameters, chosen by analysing what happens in the material during creasing and folding. Practically, the main focus will lie on quantities connected to MD and ZD, because we assume that plane stress holds in the problem, and the effects related to the CD are negligible. In order to maximise the information gained from a given number of runs, a design-of-experiments procedure as previously mentioned is used, and a regression analysis will be made on how the various parameters affect the RCS.

The simulations are performed in the finite element program Abaqus/Standard. A Python script makes up the main program, comprising a queue of numerous simulations, and the main program executes other scripts as well. These scripts will edit parameters in the model in between runs before the next one is started, and relevant, pre-selected information is stored after each run.

For every set of material parameters, two jobs are needed to calculate the RCS value, where a 'job' signifies a single simulation of the whole process. One of these jobs will run the entire creasing–folding process as described in 2.1.2; the other will skip the creasing procedure.

The trial design matrix to be used is produced by the statistical tool iSight, sampled using the optimal Latin hypercube method.

3.1 Necessary considerations

A parameter is called a *model parameter* if it enters the mathematics of the model directly, and a *testable parameter* if it is measured in industrial tests. Before executing the study, a number of challenges rise:

- Most of the testable parameters that are interesting to examine are not model parameters. Non-model parameters can not be altered directly in Abaqus; the parameters to study must be connected to model parameters by means of the theory presented.
- In some cases, several parameters may be co-dependent. The coupling is in general not simple, and ignoring this may cause some parameters to take on other values than those desired.
- Some parameters are defined implicitly and may be coupled with model parameters using theory only, and so require a series of simulated tests.
- Arbitrary parameter combinations can not be used in general, due to the material model which poses some constraints on the parameters. Specifically, for some choices, the model can not be guaranteed to fulfil the laws of thermodynamics, and for other choices, the yield surface might be definable. These pitfalls are described further in sections 3.3.1 and 3.3.3.

3.2 Parameters chosen

The model contains over 70 independent parameters. Apart from the fact that a study comprising all of these would be computationally too expensive, most of these parameters can not be interpreted intuitively nor connected to experiments performed in reality. By analyzing the processes that occur in creasing and folding, a few quantities stand out as more interesting to study, listed below.

Elastic parameters. In the creasing and folding procedure, the dominant deformation modes are normal straining (i.e. non-shearing) in MD and ZD, as well as shearing between MD and ZD.

- MD–ZD and CD–ZD shear moduli G_{13}, G_{23}
  - Although CD–ZD shearing is small in the tests, G_{23} will be altered because the model equates it with G_{13}, see (3.3)–(3.5).
- MD Young's modulus E_1
- ZD Young's modulus for tension E_{3t}
  - The elastic behaviour for paperboard is different in ZD tension and compression; the latter is handled separately.

The elasticity matrix must be symmetric, which poses a constraint on some of the parameters, namely

$$E_1\nu_{21} = E_2\nu_{12}. \tag{3.1}$$

There is one degree of freedom in specifying either E_2 or ν_{21}, which requires a rule to be imposed for uniqueness. Because ν_{21} influences the plastic behaviour, it is convenient to keep this constant, to increase the robustness of the yield function parameter calculations, and to to make the plastic behaviour independent of E_2. While it was ultimately decided to keep ν_{21} constant, some other possibilities were considered as well:

- E_2 fixed. This is a reasonable choice at first glance, but (3.1) leads to ν_{21} being determined in part by E_2, giving less robust calculations of the yield surface coefficients, which are dependent on ν_{21}, see sections 3.3.2–3.3.3.
- The product $\nu_{12}\nu_{21}$ fixed. Such a constraint is experimentally motivated in [3] and [4, Paper A, p. 14], but (3.1) shows that this would give a proportionality $E_2 \propto 1/\nu_{12}^2$, which results in large variations in E_2 for moderate variations in ν_{12}.

The numerical values that these elastic parameters take correspond to the material's approximately linear behaviour at small strains. These conventional parameters do not enter the model directly; rather, the parameters used in the model for elasticity are $A_1, \ldots, A_8$, defined in section 2.1.1.

Elasto-plastic parameters. These parameters directly affect the elastic as well as the plastic behaviour of the material. The following parameters will be studied:

- MD–CD Poisson's ratio ν_{12}
- ZD compressivity ε_C
  - This parameter is evaluated by considering a ZD compression test, defined as the absolute value of the ZD strain at a pressure of 10 MPa. In the model, this variable enters by a combination of the elastic parameters A_7 and A_8, and the hardening material constant a_7. This parameter can not be computed from theory only; instead, the three mentioned parameters will be varied to generate a curve, from which any values may be chosen. It's assumed that other parameters' influence in this test is negligible, so one such curve will be used for all materials.
  - The reason that this is regarded instead of, for example, the Young's modulus or yield stress for ZD compression is the paperboard's curious behaviour in this loading case. It has been shown that compressed paperboard will re-expand after a period of time – what looks like plasticity at first glance actually turns out to be viscoelasticity. Because the model does not account for this phenomenon, the total strain is considered, which is something measurable in physical tests and something easily interpretable.

The three parameters a_7, A_7, A_8 will be adjusted all at once in a proportional manner:

$$\begin{bmatrix} a_7 \\ A_7 \\ A_8 \end{bmatrix} = C \begin{bmatrix} a_7^* \\ A_7^* \\ A_8^* \end{bmatrix}, \quad C > 0, \tag{3.2}$$

where C is the *coefficient of compressivity*, and the starred quantities correspond to the nominal values.

Plastic parameters: initial yield stresses. The complex yield surface gives one initial yield stress value for each principal loading case, i.e. uniaxial compression and tension, as well as pure shear. The following will be considered:

- MD tension, σ_y^{MDt}
  - While the amount of CD tension and MD/CD shearing is negligible in the model, it has been found that altering the yield stresses of CD tension and 45° tension σ_y^{CDt}, $\sigma_y^{45^\circ}$ proportionally together with that of MD tension increases calculation robustness, see section 3.3.3. The 45° direction is the direction halfway between MD and CD.

- Out-of-plane shear $\sigma_y^{MD/ZD}$, $\sigma_y^{CD/ZD}$
  - Similarly, CD/ZD shearing does not occur in the tests, but it is altered to increase the robustness when determining the coefficients.
- MD compression σ_y^{MDc}
- ZD tension σ_y^{ZDt}

Other plastic parameters. The yield surface consists of more than the initial yield stresses. To complete the study, we will also consider

- Paper–paper friction parameter m
- Yield surface exponent k

All in all, this gives 11 independent parameters to study.

3.3 Connecting model parameters and testables

As stated before, most parameters that may be tested for in experiments do not enter the material model directly, so they have to be linked somehow.

3.3.1 Elastic parameters

At small deformations, the linearised elasticity matrix which connects stresses and strains is expressed in the parameters A_i in [4, Paper B, p. 9–10] as

$$\boldsymbol{D}_0 = \begin{bmatrix} 2(A_1+A_2+A_5) & A_5-2A_4 & -A_6 & & & \\ A_5-2A_4 & 2(A_2+A_4+A_5) & -A_6 & & & \\ -A_6 & -A_6 & 2A_3H^+ + 4A_7A_8H^- & & & \\ & & & A_5+A_6 & & \\ & & & & A_6 & \\ & & & & & A_6 \end{bmatrix}, \tag{3.3}$$

where blank entries stand for zeroes. The same matrix will then be expressed using the standard parameters, in order to determine the A parameters. Assuming that the Poisson's ratios between the in-plane and out-of-plane directions are zero, i.e. $\nu_{13} = \nu_{23} = \nu_{31} = \nu_{32} = 0$, the inverse is known to be

$$\boldsymbol{D}_0^{-1} = \begin{bmatrix} 1/E_1 & -\nu_{21}/E_2 & & & & \\ -\nu_{12}/E_1 & 1/E_2 & & & & \\ & & 1/E_3 & & & \\ & & & 1/G_{12} & & \\ & & & & 1/G_{13} & \\ & & & & & 1/G_{23} \end{bmatrix} \tag{3.4}$$

This matrix is block-diagonal and may be inverted analytically easily, i.e.

$$\boldsymbol{D}_0 = \begin{bmatrix} aE_1 & aE_1\nu_{21} & & & & \\ aE_2\nu_{12} & aE_2 & & & & \\ & & E_3 & & & \\ & & & G_{12} & & \\ & & & & G_{13} & \\ & & & & & G_{23} \end{bmatrix}, \tag{3.5}$$

where $a = 1/(1 - \nu_{12}\nu_{21})$. Assuming $G_{13} = G_{23}$, equating these two expressions gives a linear system to find five of the eight A_i:

$$\overbrace{\begin{bmatrix} aE_1 \\ aE_2\nu_{12} \\ aE_2 \\ G_{12} \\ G_{13} \end{bmatrix}}^{\boldsymbol{E}} = \overbrace{\begin{bmatrix} 2 & 0 & 2 & 2 & 0 \\ 0 & 0 & -2 & 1 & 0 \\ 0 & 2 & 2 & 2 & 0 \\ 0 & 0 & 0 & 1 & 1 \\ 0 & 0 & 0 & 0 & 1 \end{bmatrix}}^{\boldsymbol{M}} \overbrace{\begin{bmatrix} A_1 \\ A_2 \\ A_4 \\ A_5 \\ A_6 \end{bmatrix}}^{\boldsymbol{A}}. \tag{3.6}$$

Inverting the system (3.6) provides

$$\boldsymbol{A} = \begin{bmatrix} 0.5 & 0.5 & 0 & -1.5 & 1.5 \\ 0 & 0.5 & 0.5 & -1.5 & 1.5 \\ 0 & -0.5 & 0 & 0.5 & -0.5 \\ 0 & 0 & 0 & 1 & -1 \\ 0 & 0 & 0 & 0 & 1 \end{bmatrix} \boldsymbol{E}, \tag{3.7}$$

i.e. $(A_1, A_2, A_3, A_4, A_6)$ may be calculated, given any $(E_1, E_2, \nu_{12}, G_{12}, G_{13})$, all of which are nonzero. The inverse calculations consist of more than a single matrix multiplication, but are derived from (3.6) and (3.1) as

$$\begin{aligned} \nu_{12} &= \frac{aE_2\nu_{12}}{aE_2} = \frac{-2A_4 + A_5}{2(A_2 + A_4 + A_5)} \\ \nu_{21} &= \nu_{12}\frac{E_2}{E_1} = \nu_{12}\frac{A_2 + A_4 + A_5}{A_1 + A_4 + A_5} \\ a &= \frac{1}{1 - \nu_{12}\nu_{21}} \\ E_1 &= 2\frac{A_1 + A_4 + A_5}{a} \\ E_2 &= 2\frac{A_2 + A_4 + A_5}{a} \\ G_{12} &= A_5 + A_6 \\ G_{13} &= A_6. \end{aligned} \tag{3.8}$$

This conversion gives rise to a problem, since a reasonable parameter specification in $\boldsymbol{E}$ can give rise to *negative* A_i, which possibly results in unphysical in-plane contributions to the energy; a non-negative set of A_i is a sufficient condition for a physical model, in the sense that energy should be increasing for an arbitrary deformation [4, Paper C, p. 9]. Specifically, it is found that A_2 and A_4 pose the biggest risk of becoming negative.

Because A_2 mainly relates to CD straining, a mode that is practically absent in the simulation, A_2 is allowed to become negative without any preventive measures. On the other hand, if A_4 becomes negative for some parameter choice, it is set to 0 instead. This will influence (E_1, ν_{12}, G_{13}), meaning that this triple no longer has the values specified by the design matrix. The design matrix will be updated to reflect this, to keep the final statistical analysis coherent. Other parameters such as E_2, ν_{21} and G_{12} will be influenced as well. This is ignored, since the amount of straining in the CD is small.

From (3.3) and (3.5), the ZD initial elastic modulus is given by

$$E_3 = 2A_3H^+ + 4A_7A_8H^- \tag{3.9}$$

E_3 takes different values in a compressive and tensile domain, with the help of the switch functions H^+ and H^-; these both take on the value 0 or 1, depending on the deformation, and the functions complement each other. The parameters for the compressive domain, A_7 and A_8, will be varied independently of their tensile equivalent, A_3. For tension,

$$A_3 = \frac{E_{3t}}{2}. \tag{3.10}$$

3.3.2 Yield surface normal components

Some of the subsurfaces are sloped, to model how the material yields for arbitrary stresses. The slopes are represented by the coefficients $N_{ij}^{(\nu)}$ that appear in the yield surface, determined from [4, Paper A, p. 16]:

$$
\begin{aligned}
N_{ij}^{(1)} &= \frac{1}{\sqrt{1+{\nu_{12}}^2}} \begin{bmatrix} 1 & 0 & 0 \\ 0 & -\nu_{12} & 0 \\ 0 & 0 & 0 \end{bmatrix} \\
N_{ij}^{(2)} &= \frac{1}{\sqrt{1+{\nu_{21}}^2}} \begin{bmatrix} -\nu_{21} & 0 & 0 \\ 0 & 1 & 0 \\ 0 & 0 & 0 \end{bmatrix} \\
N_{ij}^{(9)} &= \frac{1}{\sqrt{2\cdot 0.5^2+m^2}} \begin{bmatrix} 0 & 0 & 1 \\ 0 & 0 & 0 \\ 0 & 0 & m \end{bmatrix} \\
N_{ij}^{(10)} &= \frac{1}{\sqrt{2\cdot 0.5^2+m^2}} \begin{bmatrix} 0 & 0 & -1 \\ 0 & 0 & 0 \\ 0 & 0 & m \end{bmatrix} \\
N_{ij}^{(11)} &= \frac{1}{\sqrt{2\cdot 0.5^2+m^2}} \begin{bmatrix} 0 & 0 & 0 \\ 0 & 0 & 1 \\ 0 & 0 & m \end{bmatrix} \\
N_{ij}^{(12)} &= \frac{1}{\sqrt{2\cdot 0.5^2+m^2}} \begin{bmatrix} 0 & 0 & 0 \\ 0 & 0 & -1 \\ 0 & 0 & m \end{bmatrix}
\end{aligned}
\tag{3.11}
$$

These are normed so that

$$
\operatorname{sym}\left(N_{ij}^{(\nu)}\right) : \operatorname{sym}\left(N_{ij}^{(\nu)}\right) = 1, \tag{3.12}
$$

where sym is the symmetric part operator, defined as $\operatorname{sym}(\boldsymbol{A}) = (\boldsymbol{A}+\boldsymbol{A}^T)/2$.

3.3.3 Yield stresses

The yield stress for each loading case is governed by the initial plastic distances $\tau_0^{(\nu)}$. As an example, the relation between the MD/ZD shear yield stress $\sigma_y^{MD/ZD}$ and the model parameter $\tau_0^{(9)}$ is seen in fig. 3.1; there are analogous relations between the other yield stresses and $\tau_0^{(\nu)}$. A uniaxial test for a sample cut out in the 45° direction is performed to find the yield stress for MD/CD shearing.

To couple the parameters for the uniaxial loading cases, i.e. compression and tension in MD, CD and ZD, it's assumed that only one of the stress tensor components is nonzero. For MD/ZD and CD/ZD shearing, the yield stress during a state of pure shear stress is assumed to be known from experiments, as an idealisation.

MD and CD tension. For a uniaxial MD tension test, let σ_{11}^{MDt} denote the yield stress. The stress tensor is $\sigma_{11}^{MDt}\bar{\boldsymbol{v}}_0^{(1)} \otimes \bar{\boldsymbol{v}}_0^{(1)}$. Inserting this stress state in (2.12) and setting $f = 0$ gives

$$
\left(\frac{\sigma_{11}^{MDt} N_{11}^{(1)}}{\tau_0^{(1)}}\right)^{2k} - 1 = 0, \tag{3.13}
$$

which is then solved for $\tau_0^{(1)}$. For CD tension, it's completely analogous; if yielding starts at a stress of σ_{22}^{CDt}, the stress tensor is $\sigma_{22}^{CDt}\bar{\boldsymbol{v}}_0^{(2)} \otimes \bar{\boldsymbol{v}}_0^{(2)}$ and one can solve for $\tau_0^{(2)}$ from

$$
\left(\frac{\sigma_{22}^{CDt} N_{22}^{(2)}}{\tau_0^{(2)}}\right)^{2k} - 1 = 0. \tag{3.14}
$$

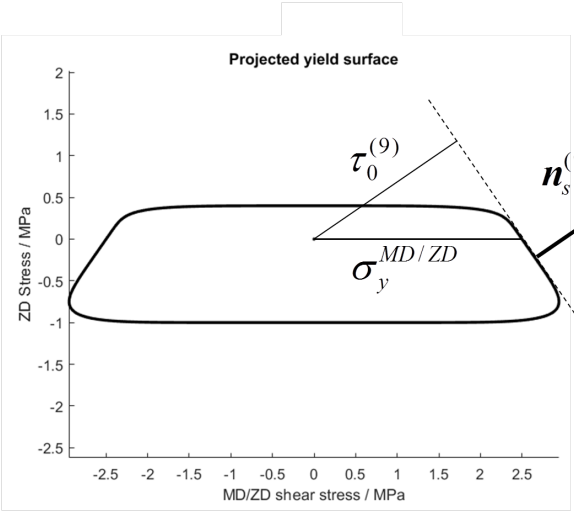

Figure 3.1: Initial yield surface projected onto the (τ_{33}, τ_{13}) plane, illustrating the quantities $\sigma_y^{MD/ZD}$, $\tau_0^{(9)}$ and $\boldsymbol{n}_s^{(9)}$.

MD and CD compression. Ideal plasticity is assumed for uniaxial loading in MD and CD. Assume that the (constant) yield stress in MD compression is σ_{11}^{MDc}. Using the stress tensor is $-\sigma_{11}^{MDc}\bar{\boldsymbol{v}}_0^{(1)} \otimes \bar{\boldsymbol{v}}_0^{(1)}$ in (2.12), $f = 0$ gives

$$\left(\frac{\sigma_{11}^{MDc} N_{11}^{(2)}}{\tau_0^{(2)}}\right)^{2k} + \left(\frac{\sigma_{11}^{MDc} N_{11}^{(4)}}{\tau_0^{(4)}}\right)^{2k} - 1 = 0, \tag{3.15}$$

which can be solved for $\tau_0^{(4)}$. For CD compression, the yield stress is assumed to be σ_{22}^{CDc}. The stress tensor is $-\sigma_{22}^{CDc}\bar{\boldsymbol{v}}_0^{(2)} \otimes \bar{\boldsymbol{v}}_0^{(2)}$, and $f = 0$ for this loading case gives

$$\left(\frac{\sigma_{22}^{CDc} N_{22}^{(1)}}{\tau_0^{(1)}}\right)^{2k} + \left(\frac{\sigma_{22}^{CDc} N_{22}^{(5)}}{\tau_0^{(5)}}\right)^{2k} - 1 = 0, \tag{3.16}$$

to be solved for $\tau_0^{(5)}$. However, there turns out to be many cases where there is no $\tau_0^{(5)} \in \mathbb{R}$ to solve this, even for reasonable parameter specifications. Because the amount of CD compression in the model is negligible, $\tau_0^{(5)}$ is set to a constant value of 21 MPa, based on [4, Paper C, p. 12].

MD–CD shear. To calibrate the MD–CD shear yield stress, a uniaxial tension test in the 45° direction is performed, because there is no known way to accomplish a pure MD–CD shear state to the point of yielding, nor anything close to it. Assume that the material yields at a stress of σ^{45t} in this test. In a coordinate system based on the 45° direction, the stress tensor looks like

$$\boldsymbol{\tau}_{45} = \sigma^{45t} \begin{bmatrix} 1 & 0 & 0 \\ 0 & 0 & 0 \\ 0 & 0 & 0 \end{bmatrix}. \tag{3.17}$$

The system is returned to the MD-based coordinate system based by applying a rotation matrix:

$$\boldsymbol{\tau} = \boldsymbol{R}^T \boldsymbol{\tau}_{45} \boldsymbol{R} = \frac{\sigma^{45t}}{2} \begin{bmatrix} 1 & 1 & 0 \\ 1 & 1 & 0 \\ 0 & 0 & 0 \end{bmatrix}, \qquad \boldsymbol{R} = \begin{bmatrix} \cos(\theta) & -\sin(\theta) & 0 \\ \sin(\theta) & \cos(\theta) & 0 \\ 0 & 0 & 1 \end{bmatrix}, \tag{3.18}$$

where $\theta = -45°$. $f = 0$ for this loading case gives

$$\left(\sigma^{45t}\frac{N_{11}^{(1)} + N_{22}^{(1)}}{2\tau_0^{(1)}}\right)^{2k} + \left(\sigma^{45t}\frac{N_{11}^{(2)} + N_{22}^{(2)}}{2\tau_0^{(2)}}\right)^{2k} + \left(\sigma^{45t}\frac{N_{12}^{(3)} + N_{21}^{(3)}}{2\tau_0^{(3)}}\right)^{2k} - 1 = 0, \tag{3.19}$$

which can be solved for $\tau_0^{(3)}$. Note that $N_{12}^{(3)} = N_{21}^{(3)}$. This method has also been used in [8, p. 40].

ZD compression. Let σ_{33}^{ZDc} be the yield stress in a compression test. The stress tensor is $\sigma_{33}^{ZDc}\bar{\boldsymbol{v}}_0^{(3)} \otimes \bar{\boldsymbol{v}}_0^{(3)}$. Setting $f = 0$ then gives

$$\left(\frac{\sigma_{33}^{ZDc} N_{33}^{(7)}}{\tau^{(7)}} \right)^{2k} - 1 = 0, \tag{3.20}$$

to be solved for $\tau_0^{(7)}$.

MD–ZD and CD–ZD shear. Assume that the yield stress in a pure MD–ZD shear state is $\sigma_{13}^{MD/ZD}$. The stress tensor is $\sigma_y^{MD/ZD}(\bar{\boldsymbol{v}}_1 \otimes \bar{\boldsymbol{v}}_3 + \bar{\boldsymbol{v}}_3 \otimes \bar{\boldsymbol{v}}_1)$ and setting $f = 0$ gives

$$\left(\frac{\sigma_{13}^{MD/ZD} N_{13}^{(9)}}{\tau_0^{(9)}} \right)^{2k} - 1 = 0, \tag{3.21}$$

which is then solved for $\tau_0^{(9)}$. The behaviour and yield strength is assumed to be the same in CD–ZD shear as in MD–ZD shear, $\tau_0^{(10)}, \ldots, \tau_0^{(12)}$ are set equal to $\tau_0^{(9)}$ due to symmetry.

ZD tension. Let σ_{33}^{ZDt} be the yield stress in the uniaxial ZD tension test. The stress tensor is then $\sigma_{33}^{ZDt}\bar{\boldsymbol{v}}_0^{(3)} \otimes \bar{\boldsymbol{v}}_0^{(3)}$.

$$\sum_{i=8}^{12} \left(\frac{\sigma_{33}^{ZDt} N_{33}^{(i)}}{\tau_0^{(i)}} \right)^{2k} - 1 = 0. \tag{3.22}$$

Because $N_{33}^{(9)} = N_{33}^{(i)}$ and $\tau_0^{(9)} = \tau_0^{(i)}$ for $i \in \{10, 11, 12\}$, it simplifies to

$$\left(\frac{\sigma_{33}^{ZDt} N_{33}^{(8)}}{\tau_0^{(8)}} \right)^{2k} + 4 \left(\frac{\sigma_{33}^{ZDt} N_{33}^{(9)}}{\tau_0^{(9)}} \right)^{2k} - 1 = 0, \tag{3.23}$$

which finally may be solved for $\tau_0^{(9)}$. The formulae for calculating every $\tau_0^{(\nu)}$ are summarised in table 3.1, and one can see that $\tau_0^{(3)}$, $\tau_0^{(4)}$ and $\tau^{(8)}$ become nonreal for certain material parameter set, thus making these sets unusable. This is taken into account when choosing the values that every parameter should assume.

3.3.4 Compressivity calibration

To find ε_C as a function of C, both introduced in section 3.2, individual values on the function are computed, each from one compression test for some C value, and then fit these points to a curve. The ZD compression parameters will be adjusted by scaling them by C with respect to their nominal values. After retrieving the data points, they are interpolated linearly to complete the curve. The result is shown in fig. 3.2.

3.3.5 Summary

All the parameters to be studied have now been expressed in terms of model parameters, and the relations are summarised in table 3.2.

Table 3.1: Calculation of every $\tau_0^{(\nu)}$.

ν	Loading case	$\tau_0^{(\nu)} =$
1	MD tension	$N_{11}^{(1)}\sigma_{11}^{MDt}$
2	CD tension	$N_{22}^{(2)}\sigma_{22}^{CDt}$
3	MD/CD shear (positive)	$\sigma^{45t}\left(N_{12}^{(3)}+N_{21}^{(3)}\right)\left(1-\sum_{i=1}^{2}\left(\sigma^{45t}\frac{N_{11}^{(i)}+N_{22}^{(i)}}{2\tau_0^{(i)}}\right)^{2k}\right)^{\frac{-1}{2k}}$
4	MD compression	$\left\lvert N_{11}^{(4)}\right\rvert \sigma_{11}^{MDc}\left(1-\left(\frac{\sigma_{11}^{MDc}N_{11}^{(2)}}{\tau_0^{(2)}}\right)^{2k}\right)^{\frac{-1}{2k}}$
5	CD compression	21 MPa
6	MD/CD shear (negative)	$\tau_0^{(3)}$
7	ZD compression	$\sigma_{33}^{ZDc}\left\lvert N_{33}^{(7)}\right\rvert$
9	MD/ZD shear (positive)	$N_{13}^{(9)}\sigma_{13}^{MD/ZD}$
10	MD/ZD shear (negative)	$\tau_0^{(9)}$
11	CD/ZD shear (positive)	
12	CD/ZD shear (negative)	
8	ZD tension	$\sigma_{33}^{ZDt}N_{33}^{(8)}\left(1-4\left(\frac{\sigma_{33}^{ZDt}N_{33}^{(9)}}{\tau_0^{(9)}}\right)^{2k}\right)^{\frac{-1}{2k}}$

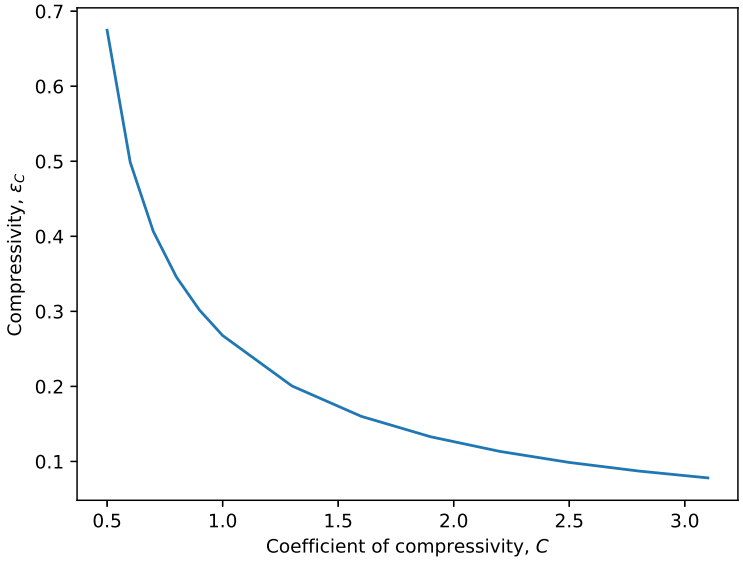

Figure 3.2: ZD compressivity curve, linearly interpolated.

Table 3.2: Summary of connections between accessible and inaccessible parameters.

Parameter(s) to study	Corresponding model parameters
E_1	A_1, A_2, A_4, A_5, A_6
G_{13}, G_{23}	
E_{3t}	A_3
k	
m	$N_{ij}^{(9)}$, ..., $N_{ij}^{(12)}$
ν_{12}	$N_{ij}^{(1)}$, A_1, A_2, A_4, A_5
σ_y^{MDt}	$\tau_0^{(\nu)}$
σ_y^{MDc}	
σ_y^{ZDt}	
$\sigma_y^{MD/ZD}$	
ε_C	a_7, A_7, A_8

3.4 Program structure

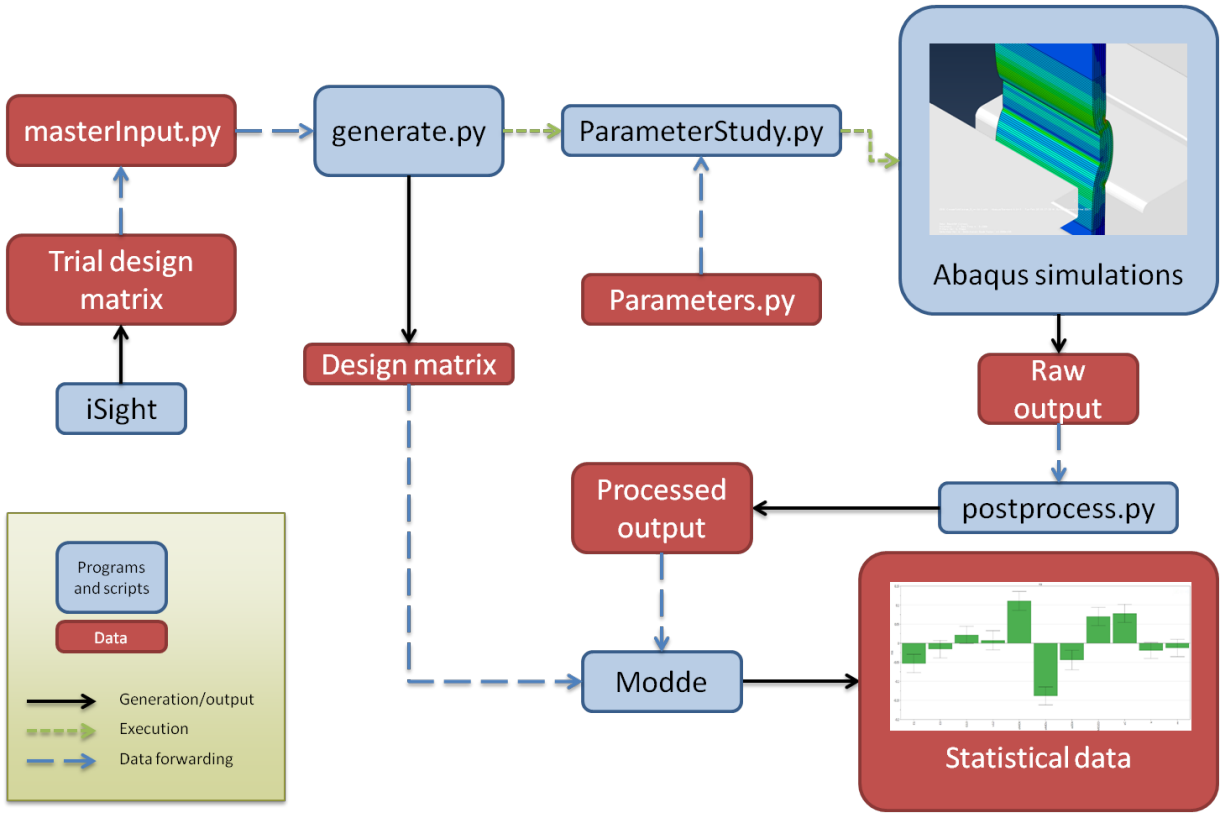

Figure 3.3: Program structure.

For the study to run smoothly, we take advantage of the Python-based scripting framework available for Abaqus/Standard. Most of the programming work consists of providing a wrapper interacting with Abaqus in different ways. The file `generate.py` starts the run. It reads from another file `masterInput.py`, which sends instructions on filenames, and specifics such as the design matrix, which is stored as text and read from another file.

Having gathered the design matrix, it then reads from another file, `Parameters.py`. Among other things, it contains the class `ParameterLibrary` which holds information on all parameters to study and the ranges they will assume. It also handles cases where a potential material model is unphysical. Another file, `ParameterStudy.py`, is responsible for connecting the information to use in Abaqus. In this file, the method `creaseUncrease()` is called to examine a single material, consisting of one creased and one uncreased run, either of which may be disabled if desired.

`creaseUncrease()` calls `setupFile()` which edits the input file name to include the material's ID, indicated by a number equal to the corresponding row in the design matrix, counting from 0. It alters the material in addition and creates two job objects: one for the creased case and another for the uncreased. The jobs are named to include the ID, and with a 'C' appended for the creased case, or a 'U' for the uncreased. The names of the output files will reflect that of the jobs, automatically handled by Abaqus. Because model files are saved, they can later be inspected for debugging purposes. `setupFile()` is written out in listing 3.1.

There are numerous methods implemented with the purpose of altering the model parameters to reflect the specification for each run, including taking care of potential disallowed parameter configurations, in which case the methods also update the design matrix accordingly. After all of this, a single simulation is started with `singleRun()`, which modifies the model to reflect whether it should be creased or not, and then submits the job to Abaqus. The output of the creased and uncreased jobs are saved together, in order to easily calculate the RCS afterward.

A .odb output database file is saved whenever a simulation fails, for instance due to convergence error, to make it easier to diagnose.

```
def setupFile(id,designMatrixRow,nameData,jobFlag=True):
  modelFileNameDefault,modelName,jobNameDefault,materialName,designMatrixUpdate = nameData

  def Id(name):
    return name + (str(id) if jobFlag else "")

  modelFileName = Id(modelFileNameDefault)

  if jobFlag:
    directory = os.getcwd()
    if os.path.exists(modelFileName+'.cae'):
      os.remove(modelFileName+'.cae')
    # Copies the model file, if the copy does not exist.
    shutil.copy(modelFileNameDefault+'.cae',modelFileName+'.cae')

  openMdb(modelFileName+'.cae') #Opens the model file.
  global model
  model = mdb.models[modelName]
  assembly = model.rootAssembly
  if jobFlag:
    jobName = Id(jobNameDefault)
    jobNames = {}
    for creaseFlag in [True,False]:
        # Creates one creased and one uncreased job and labels them accordingly.
      nextJobName = jobName + ('C' if creaseFlag else 'U')
      mdb.Job(name=nextJobName, objectToCopy=mdb.jobs[jobNameDefault])
      jobNames[creaseFlag] = nextJobName

    # Changes some of the parameters and updates this row of design matrix, if the values are inappropriate.
    # The new parameter set is stored in designMatrixRow.
  abaqusParameters,designMatrixRow = updateDesignMatrixRow(designMatrixRow,nameData)
  setAbaqusParameters(modelName,materialName,abaqusParameters)

  # Saves the file.
  mdb.save()

  return jobNames,designMatrixRow
```

Listing 3.1: Example of Python code used in the work. `setupFile()` is a function which copies an Abaqus model file and prepares the copy for simulation jobs by editing material parameters and creating job objects.

The overlaying program structure is schematically laid out in fig. 3.3.

3.5 Parameter ranges

The values that the parameters will take during tests must be decided. Every parameter will have an associated nominal value, and this default value will be multiplied by a factor within given interval in

conjunction with every simulation. A generous range of $[0.3, 2]$ is initially considered for every parameter, despite the possibility that all values in this range might not be realistic for actual paperboard. Unfortunately, some parameter combinations evidently result in incomputable yield coefficients, hypothesised to correspond to a situation wherein the sub-surfaces intersect in the wrong way, and not like a "hyper-hexahedron" as expected. Section 3.3.1 also discussed that one may encounter elastic parameters that become negative, possibly giving an unphysical model.

Before starting the series of tests, all combinations of parameters at their extremes are tested to see if they can be used without problems such as negative A_i or incomputable yield surfaces. If there are problems, it means that the parameter ranges have to be constrained further, which is done through theory by studying what part of the calculation goes wrong, and the theoretical approach is completed by trial and error. The final values are contained in table 3.3.

Table 3.3: Nominal values and ranges of parameters.

Parameter(s)	Nominal	Multipliers		Values	
		Min.	Max.	Min.	Max.
E_1	6147 MPa	0.72	2	4426 MPa	12290 MPa
σ_y^{MDt}, σ_y^{CDt}, $\sigma_y^{45°}$	22, 12, 14 MPa	0.45	2	9.9, 5.4, 6.3 MPa	44, 24, 28 MPa
σ_y^{MDc}	29 MPa	0.3	1.6	8.7 MPa	46.4 MPa
σ_y^{ZDt}	0.4 MPa	0.3	1.6	0.12 MPa	0.64 MPa
$\sigma_y^{MD/ZD}$, $\sigma_y^{CD/ZD}$	2.5 MPa	0.6	1.8	1.5 MPa	4.5 MPa
k	3	1/3	5/3	1	5
ν_{12}	0.385	0.5	1.5	0.193	0.578
m	0.7	0.3	1.6	0.21	1.12
E_{3t}	56.8 MPa	0.3	2	17.0 MPa	114 MPa
G_{13}, G_{23}	70.2 MPa	0.6	2	42.1 MPa	140 MPa
ε_C	0.2678	0.6	2	0.161	0.536

Note: k only takes integer values.

4 Postprocessing

The results from the simulations can not be used immediately, and have to be processed first. The paperboard used in the simulations has a width of 3 mm, while samples used in real tests have a width of 38 mm. In order to make these comparable, we assume that plane stress holds, and rescale all the measured forces by 38/3.

4.1 Numerical tools

A number of numerical operations are required to prepare the output data for analysis. Minor unsystematic errors such as fluctuations are often present, and curves generally have to be smoothed in order to calculate derivatives accurately.

4.1.1 Curve smoothing

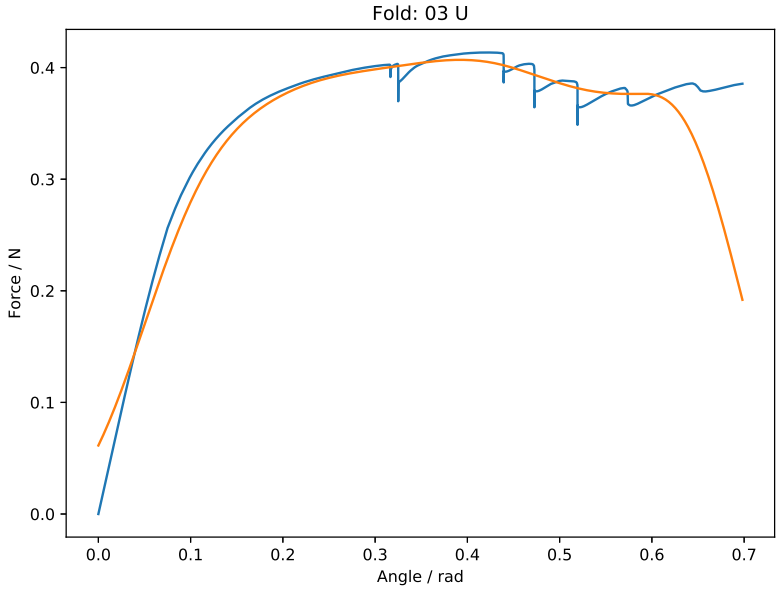

Figure 4.1: Example comparison of a raw output folding curve (blue) and corresponding smoothed (orange).

It is found that some of the folding curves exhibit discontinuities, meaning that the force might vary considerably even if measured at two angles near each other, see fig. 4.1. These discontinuities are related to the formation of wrinkles, and are a source of unsystematic errors. To handle the discontinuities, the curve F is smoothed into $\bar{F}$ by a convolution:

$$\bar{F}(\theta) = \frac{\int_{\theta_0}^{\theta_1} F(s) h_w(\theta - s) ds}{\int_{\theta_0}^{\theta_1} h_w(s) ds}, \tag{4.1}$$

where h_w is the Hann function of width w, centered at $\theta = 0$:

$$h_w(\theta) = \begin{cases} \cos^2\left(\frac{\pi}{w}\theta\right) & \text{if } |\theta| < \frac{w}{2} \\ 0 & \text{otherwise.} \end{cases} \tag{4.2}$$

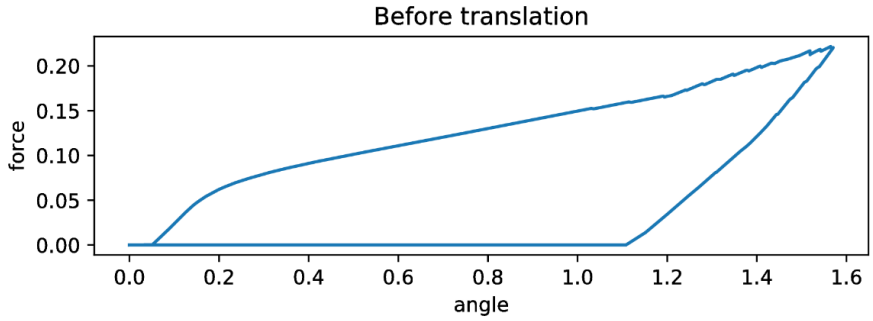

Figure 4.2: Example of a force curve during folding, showing a zero force even after the clamps have begun to rotate.

This function is chosen because of its bell shape, smoothly descending to zero when approaching $\pm w/2$. The curve to be smoothed must be judged in terms of how severe its discontinuities are, before an appropriate width of the smoothing function is chosen. Other smoothing methods were considered:

- Integrating around the desired point and dividing by the width of the integrated interval, equivalent to convolution with a pulse. This is disregarded because quite large intervals were required to make the curve smooth.
- A smoothing method by averaging was also considered, but it is disregarded because the varying density of the data points will influence the result, which is undesirable since density of data points is not an intrinsic property of the underlying curve.

To compute the convolution, the (θ, F) curve is re-sampled to evenly spaced θ by linear interpolation and the integral is approximated by a Riemann sum:

$$\bar{F}(\theta) \approx \frac{\sum_{i=0}^{n} F(\hat{\theta}_i) h_w(\theta - \hat{\theta}_i)}{\sum_{i=0}^{n} h_w(\hat{\theta}_i)}, \tag{4.3}$$

where $\hat{\theta}_i$ are the $n+1$ evenly sampled θ points. An example result of smoothing is seen in fig. 4.1.

4.1.2 Approximating derivatives

Some of the output data requires computing derivatives. Let $\hat{\theta}_i$ be evenly sampled θ points, and let $F_i = F(\hat{\theta}_i)$. The θ-derivatives of F will be approximated using central differences:

$$\left.\frac{\partial F(\theta)}{\partial \theta}\right|_{\theta=\hat{\theta}_i} \approx \frac{F_{i+1} - F_{i-1}}{2h}, \tag{4.4}$$

$$\left.\frac{\partial^2 F(\theta)}{\partial \theta^2}\right|_{\theta=\hat{\theta}_i} \approx \frac{F_{i+1} + F_{i-1} - 2F_i}{h^2}, \tag{4.5}$$

where h is the grid spacing; $\hat{\theta}_i - \hat{\theta}_{i-1} = h$ for any i. The method will be used for differentiating F as well as $\bar{F}$.

4.2 Folding forces and RCS

Due to the experimental set-up, there might be contact between the load cell and paper before folding has started; conversely, it's also possible that the clamp will rotate slightly without getting in contact with

the load cell; see fig. (4.2). These scenarios will result in a non-zero force for a zero angle, or vice versa. Because of this, the graph has to be translated such that the curve takes off at the origin.

After forcing the curve to the origin, it is smoothed through convolution according to (4.3), with $w = \theta_1/5$ for the curves of creased tests, and $w = \theta_1/3$ for the uncreased ones. A larger width is chosen for the uncreased tests due to their greater tendency of discontinuities. After smoothing, the values within $w/2$ from the endpoints θ_0 and θ_1 become useless as a consequence of the convolution, which must be kept in mind. The maximum force for each case within an interval $[0, \theta^*]$ is extracted. The RCS is then found by this force for the uncreased curve, divided by that of the creased.

The maximum folding forces for creased and uncreased samples will be denoted by $F_{f,c}$ and $F_{f,u}$, respectively. The limit angle is $\theta^* = 30° \approx 0.52\,\text{rad}$, as mentioned in section 1.

4.3 Folding slope

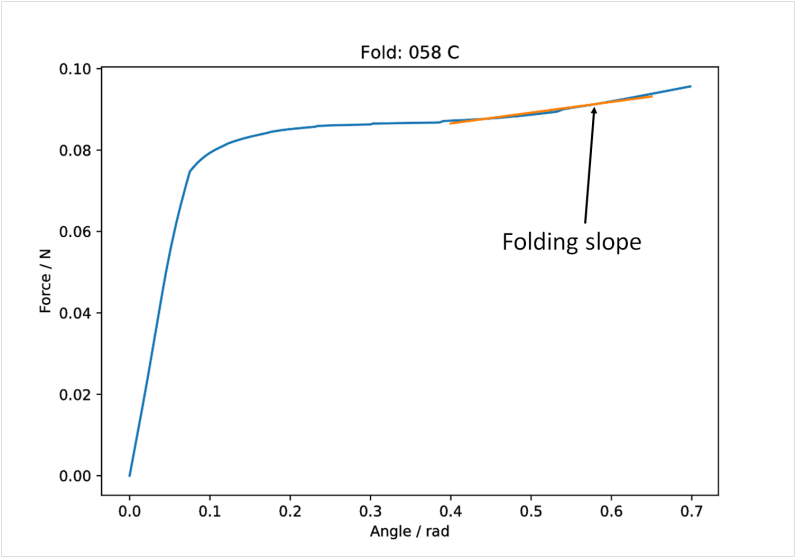

Figure 4.3: Fitting a linear polynomial (orange) to find the slope of the folding curve for a creased sample (blue).

The slope of the creased folding curve is found by sampling all (θ, F) such that $\theta \in [0.4, 0.65]$, and fitting a first-degree polynomial to this data set by the least-squares method. The folding slope, denoted s_f, is then chosen as the slope of this polynomial, see fig. 4.3.

4.4 Maximum creasing force and crease slope

The maximum creasing force is denoted by F_c and is taken as the maximum of the force during creasing. The derivative of the displacement–force curve during creasing is approximated by (4.4). While the curve is not particularly smooth, as demonstrated in fig. 4.5 which shows the derivative computed for the force curve in fig. 4.4, it succeeds in identifying the slope's minimum value s_c.

4.5 Pivoting angle

The pivoting angle, θ_P, is defined as the angle during folding at which the curvature of the curve (θ, F) is maximal. Curvature is a geometrical quantity, which can not be measured in a plane of two differently-dimensioned quantities. With respect to a scaling factor q, the q-curvature κ_q is defined as

$$\kappa_q(\theta) = \frac{\left|\frac{\partial^2 F}{\partial \theta^2}/q\right|}{\left(1 + \left(\frac{\partial F}{\partial \theta}/q\right)^2\right)^{3/2}} \tag{4.6}$$

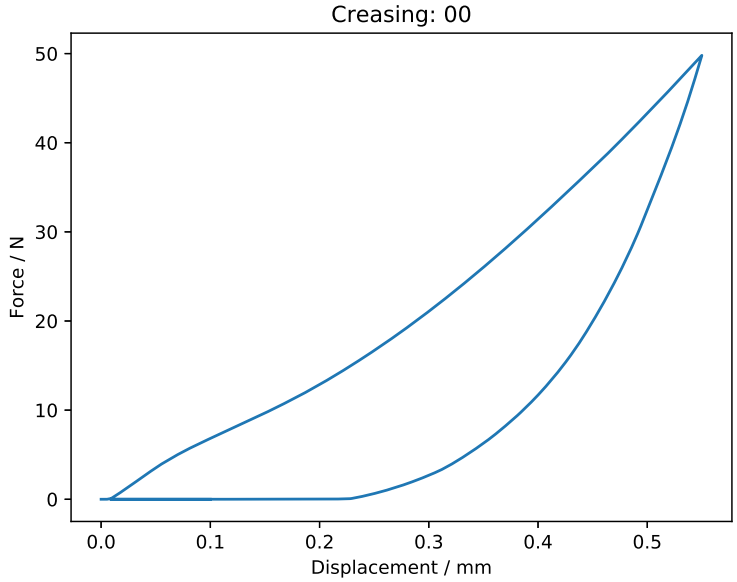

Figure 4.4: Example of a displacement–force curve during creasing.

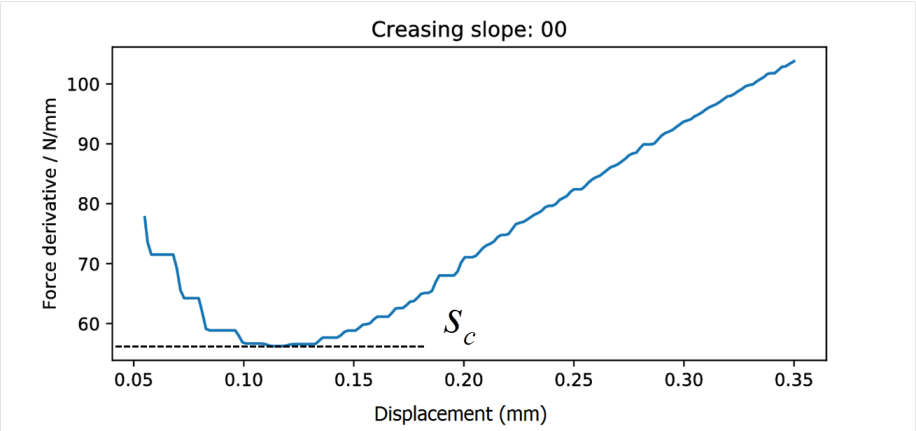

Figure 4.5: Derivative of the curve in fig. 4.4, computed using central differences, demonstrating the crease slope s_c.

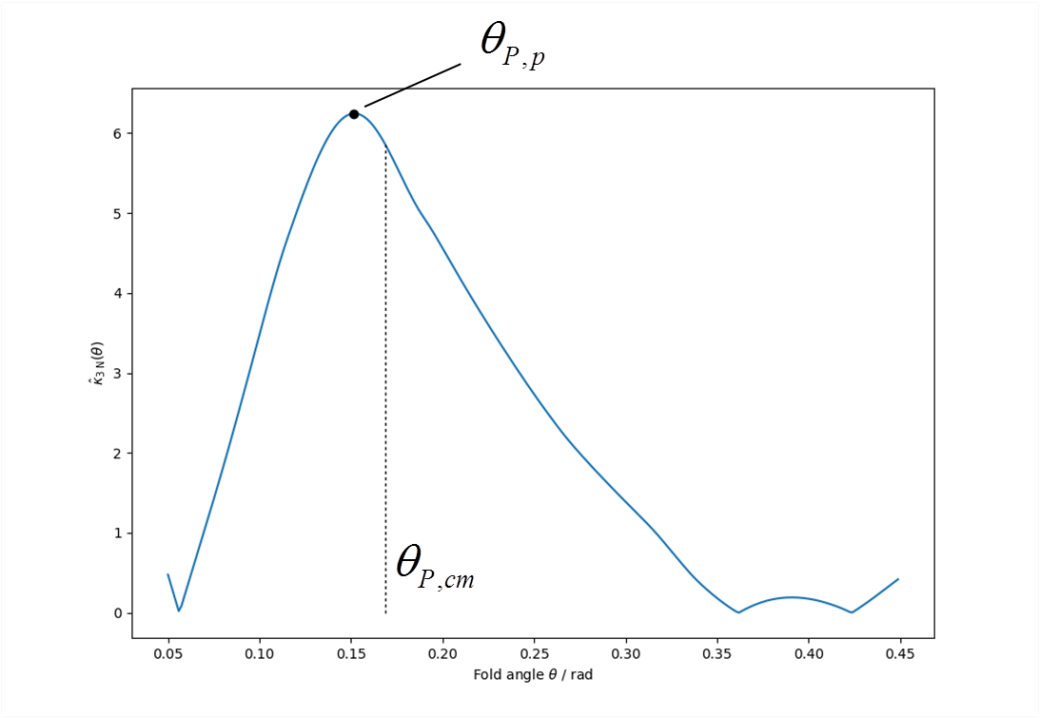

Figure 4.6: Example of a curvature graph. The black dot shows the position of $\theta_{P,p}$, and the dotted line is $\theta = \theta_{P,cm}$.

The derivatives are approximated using (4.4)–(4.5), after smoothing F according to (4.3) with $w = \theta_1/5$. Two different measures of the pivoting angle will be examined. Let $I_P = [\theta_i, \theta_f]$ be an interval limited to a region containing the maximum curvature. Inspection of the curves has shown that $I_P = [0.05, 0.45]$ is an appropriate choice; a neighbourhood around $\theta = 0$ is excluded, because derivative estimation is unreliable here. Note that this is dependent on the choice of q, see fig. 4.8, especially if there's not a well-defined plateau in the curve.

For a given q, the *peak pivoting angle* is defined by

$$\theta_{P,p} = \operatorname*{argmax}_{\theta \in I_P} \kappa_q(\theta), \tag{4.7}$$

Because argmax is not a continuous function, the choice of curvature measure may give markedly different results for two similar curves if, for instance, there are two competing 'bumps' far away from each other. An alternative is given by the *center-of-mass pivoting angle*, defined as

$$\theta_{P,cm} = \frac{\int_{\theta_i}^{\theta_f} \hat{\kappa}_q(\theta)^2 \theta \; d\theta}{\int_{\theta_i}^{\theta_f} \hat{\kappa}_q(\theta)^2 \; d\theta}, \tag{4.8}$$

which uses a shifted curvature function

$$\hat{\kappa}_q(\theta) = \kappa_q(\theta) - \min_{\theta \in I_P} \kappa_q(\theta).$$

This definition has the advantage of being continuous: a small change in the curvature function will not lead to a dramatic change in $\theta_{P,cm}$. $\theta_{P,cm}$ can be interpreted as the θ coordinate of the 'center of mass' for the curve $\left(\theta, \hat{\kappa}_q(\theta)^2\right)$ for some q.

After inspecting curvature graphs for different scaling factors, 3 N is found to be an appropriate choice of scaling factor. An example of the two curvature measures is seen in fig. 4.6. The curvature peaks at different points depending on the choice of scaling factor, illustrated in fig. 4.8, which shows the curvature of the force curve in 4.7 for different scaling factors.

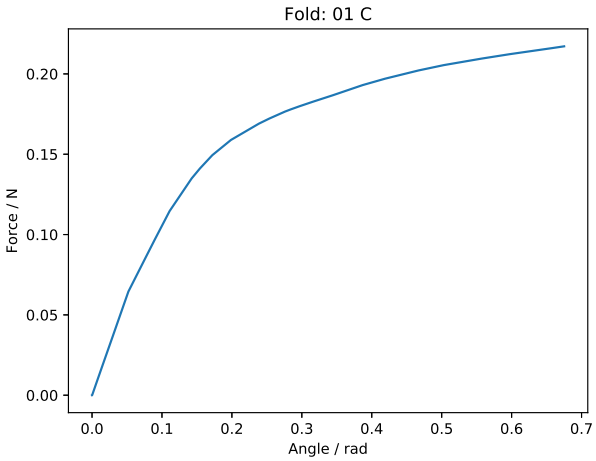

Figure 4.7: Example of a force curve for folding with no well-defined turning point, obtained through simulation.

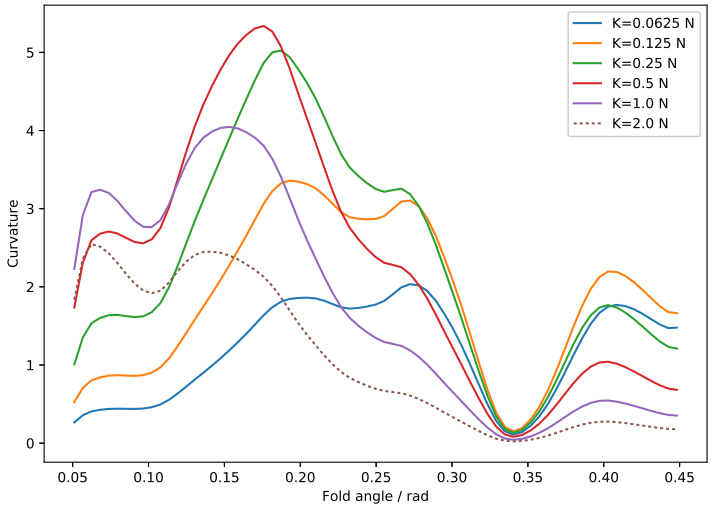

Figure 4.8: Curvature $\kappa_K(\theta)$ for the curve in (4.7), for different K.

5 Results

The effects from the parameters on every response considered have been computed by analysing the simulation output data in MODDE. The effects for the linearly modelled responses are plotted in figures 5.1–5.8. In every plot, the effects are represented by bars, and the 'whiskers' associated with a bar illustrate the 95% confidence interval. The bars are colour-coded to represent its level of significance: for any coefficient c relative to its margin of error Δ, the effect estimate is classified as very significant ($c/\Delta \geq 3$), significiant ($1 \leq c/\Delta < 3$), or insignificant ($c/\Delta \leq 1$), and the bar representing the effect is coloured green, yellow or grey, respectively.

The label meanings are specified in table 5.1. Some results that do not directly contribute to the main goals intended to establish in this thesis are left out here, instead put in the appendix in the end of this report.

Table 5.1: Text-based labels for parameters.

Quantity	Label
E_1	E1
σ_y^{MDt}	σMDt
σ_y^{MDc}	σMDc
σ_y^{ZDt}	σZDt
$\sigma_y^{MD/ZD}$	σMDZD
k	k
ν_{12}	ν12
m	m
E_{3t}	E3
G_{13}	G13
ε_C	εC

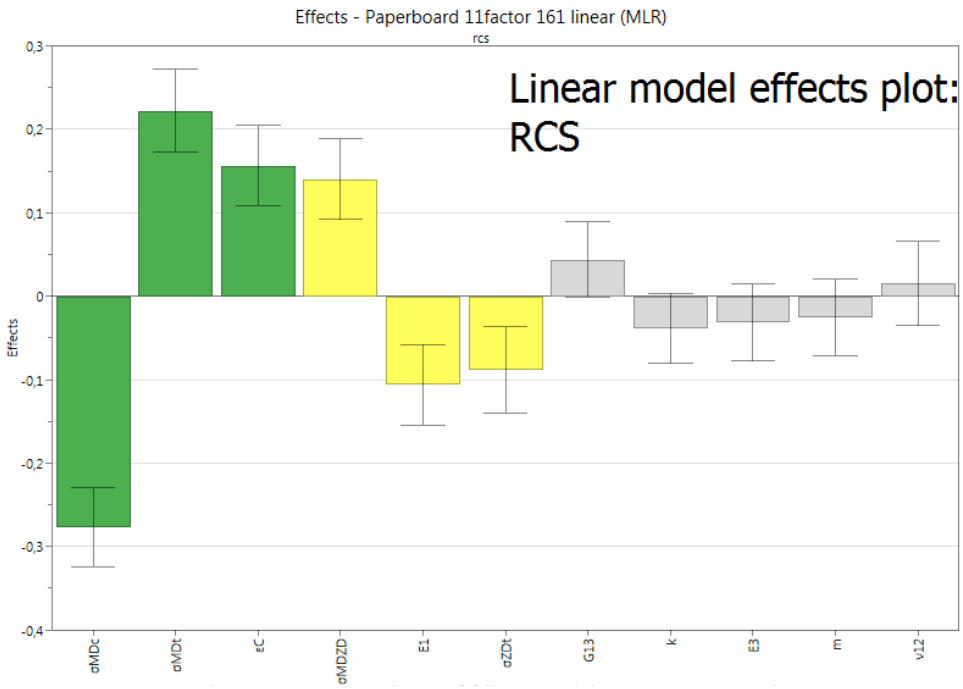

Figure 5.1: Effect plot for RCS.

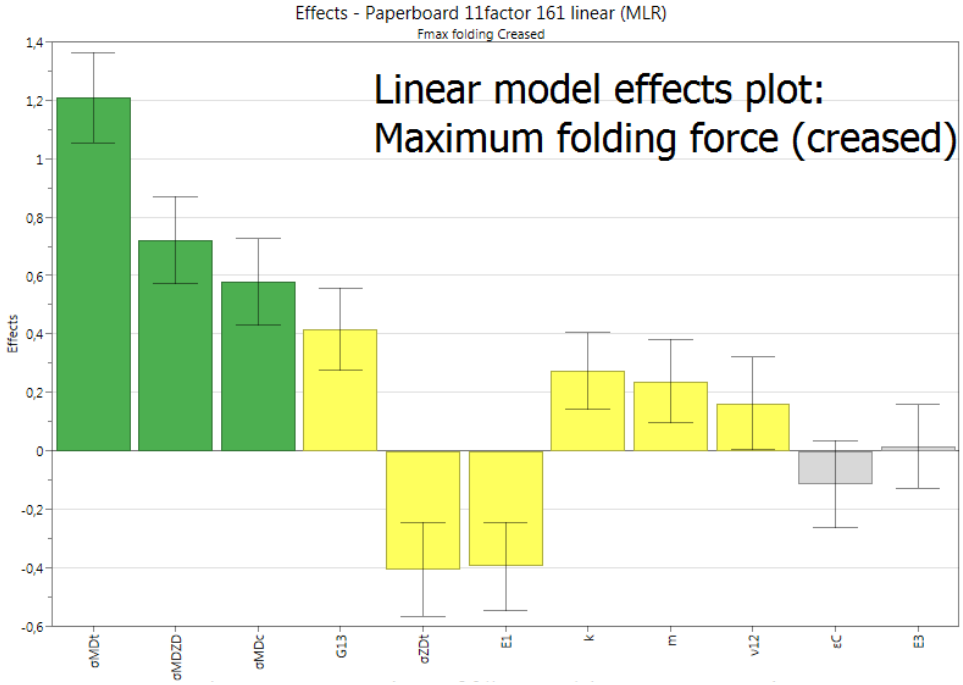

Figure 5.2: Effect plot for $F_{f,c}$.

Figure 5.3: Effect plot for $F_{f,u}$.

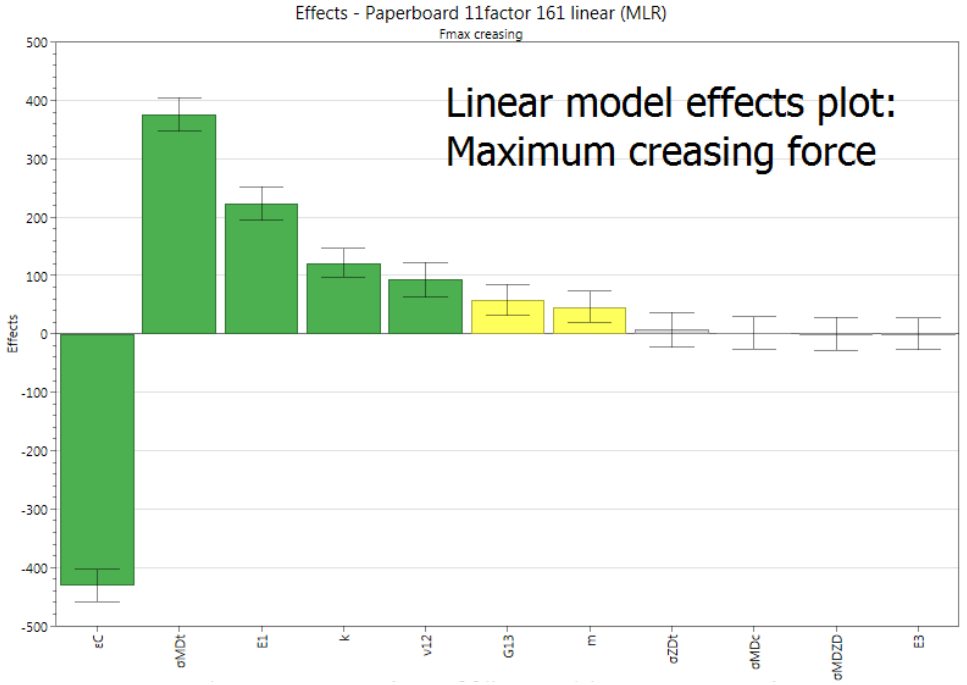

Figure 5.4: Effect plot for F_c.

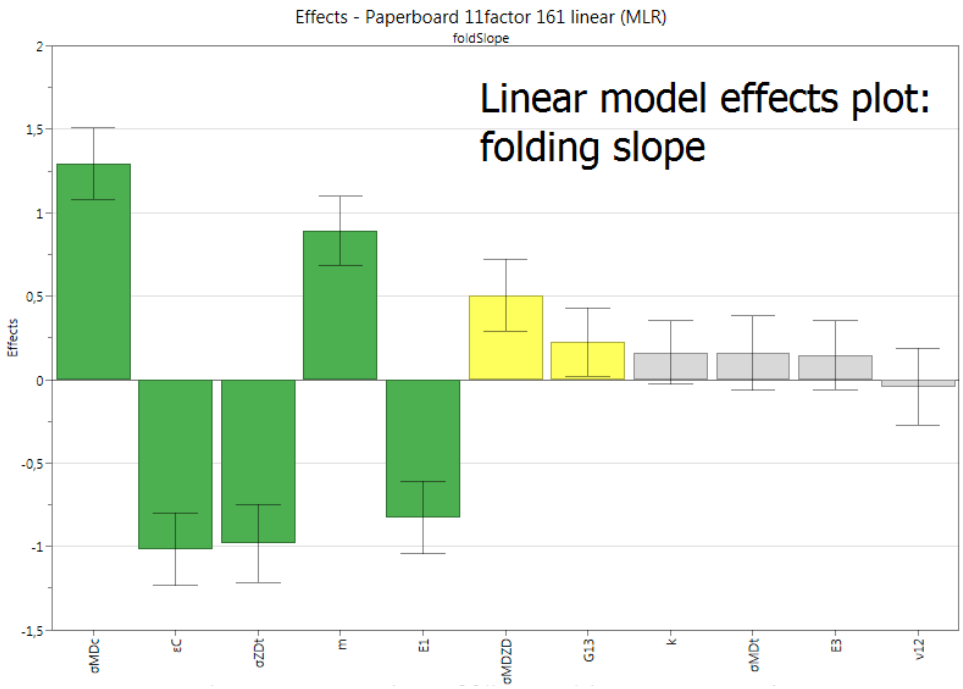

Figure 5.5: Effect plot for s_f.

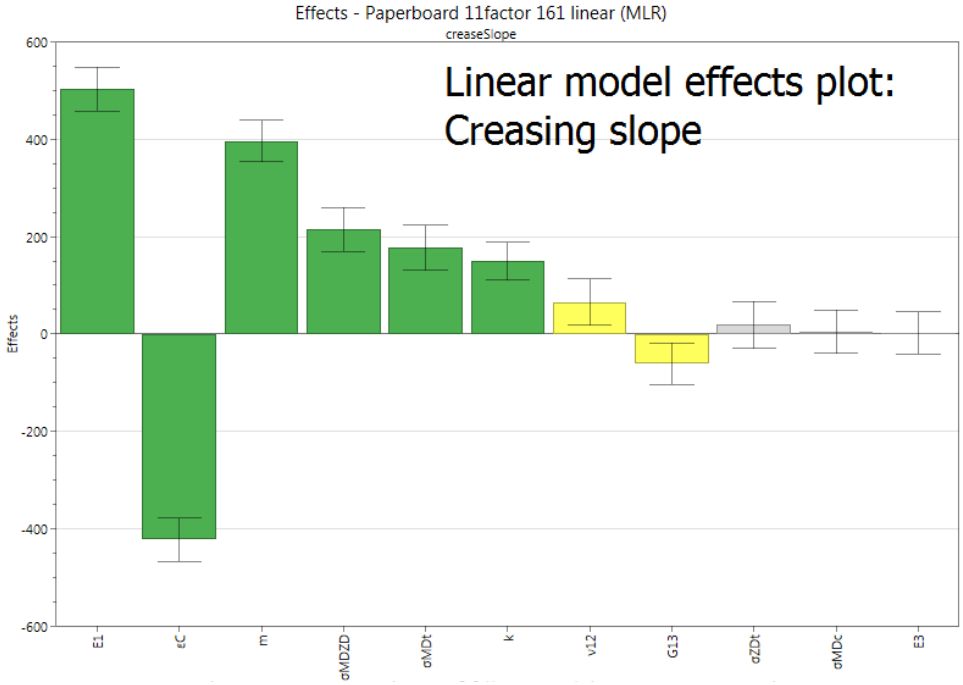

Figure 5.6: Effect plot for s_c.

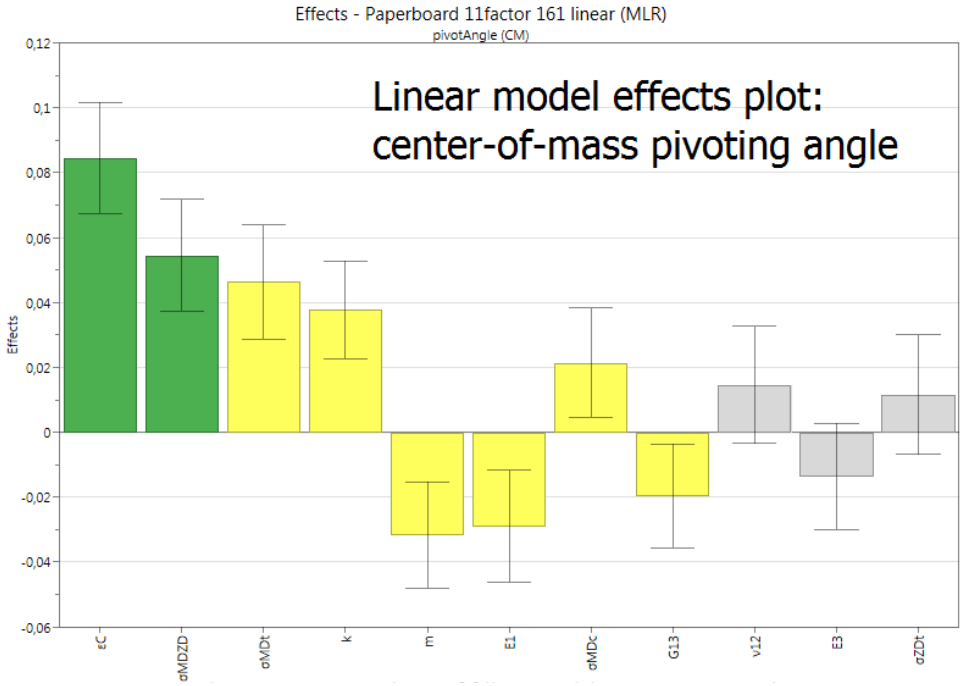

Figure 5.7: Effect plot for $\theta_{P,cm}$.

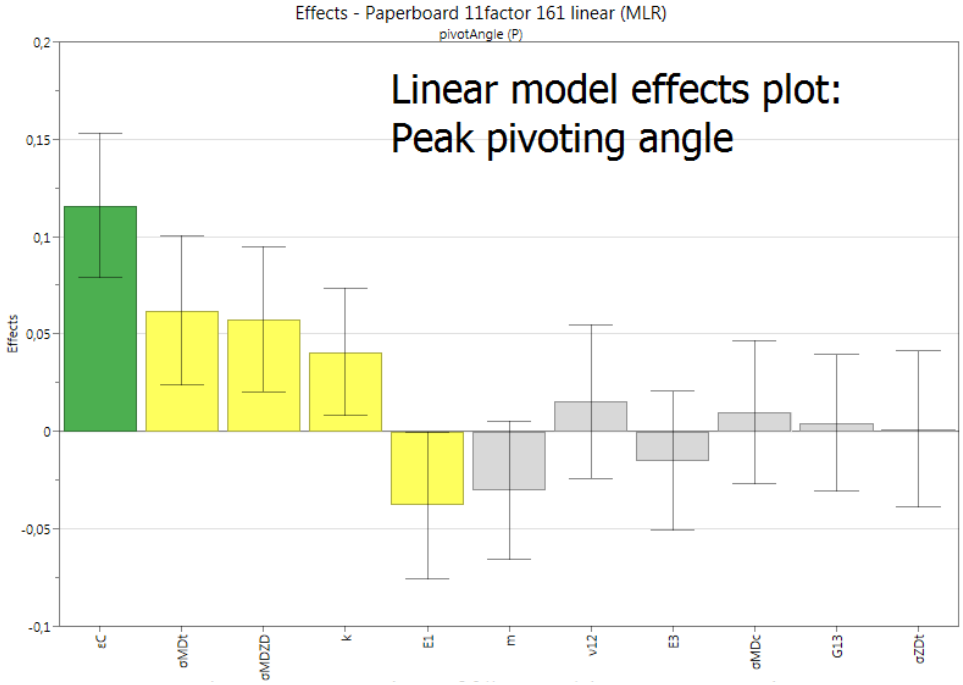

Figure 5.8: Effect plot for $\theta_{P,p}$.

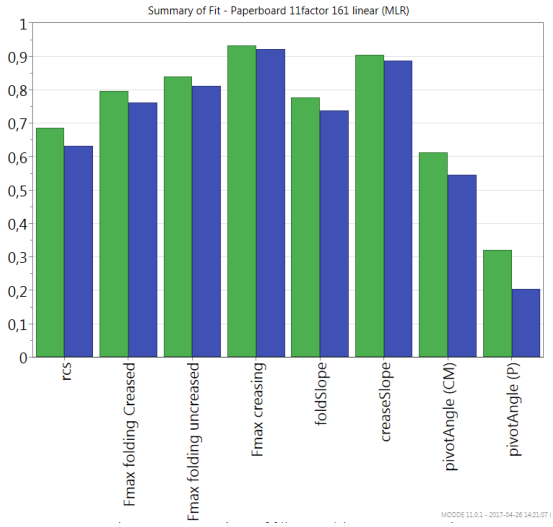

Figure 6.1: R^2 (green) and Q^2 (blue) for the linear models of RCS, $F_{f,c}$, $F_{f,u}$, F_c, folding slope, creasing slope, $\theta_{P,cm}$ and $\theta_{P,p}$.

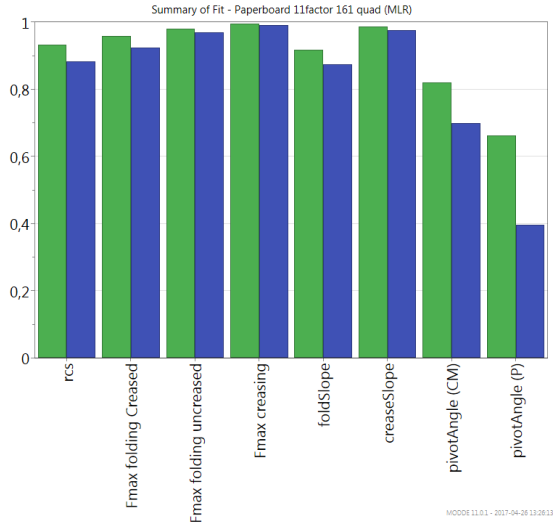

Figure 6.2: R^2 (green) and Q^2 (blue) for the quadratic models of of RCS, $F_{f,c}$, $F_{f,u}$, F_c, s_f, s_c, $\theta_{P,cm}$ and $\theta_{P,p}$.

6 Analysis

Figures 5.1–5.8 indicate that the out-of-plane tension stiffness E_{3t} does not contribute significantly to any of the responses for the linear models chosen. However, it does give some small but statistically significant linear and interactional terms in the quadratic regression models for F_c and $\theta_{P,cm}$, as seen in section A.7. The model-only parameter k has a significant effect on most responses. Because its value is an arbitrary natural number, there is freedom to choose its value so that the model corresponds to experiments better.

6.1 Summary of fit

The summary of the fit for the linear and quadratic regression models is graphed in terms of R^2 and Q^2 in figures 6.1 and 6.2, displaying these values for every modelled response. Fig. 6.1 shows that all linearly modelled responses except $\theta_{P,p}$ have $Q^2 \in [0.5, 0.95]$, indicating good models. For the quadratic models, fig. 6.2 shows that the same responses modelled quadratically have $Q^2 \in [0.65, 1]$, pointing to even more accurate models. To emphasize, R^2 is a summary of how well the values predicted using the regression model correspond to the measured ones; these data sets are plotted in figures A.2–A.3.

From fig. 6.1, it seems that $\theta_{P,cm}$ is a more robust measure of the pivoting angle than $\theta_{P,p}$ in terms of R^2 and Q^2. This is suspected to be related to the discontinuity of the argmax function, used to determine $\theta_{P,p}$. The pivoting angles measured in the experimental curve in fig. A.1 are $\theta_{P,cm} = 0.126\,\text{rad}$, $\theta_{P,p} = 0.102\,\text{rad}$. The disparity between the two measures is illustrated in fig. A.4, which does not show anything close to a 1-to-1 correlation. Because the tools used could not model $\theta_{P,p}$ very well, unlike all the other responses, this parameter has been disregarded in some of the analyses.

6.2 Response analysis

The primary factors affecting every response is tabulated in table 6.2. The most important factor affecting the RCS is σ_y^{MDc}; other important factors in descending order are σ_y^{MDt}, ε_C, $\sigma_y^{MD/ZD}$, E_1 and σ_y^{ZDt}.

Because the model often overestimates the folding slope as compared to experimental measurements, which show a near-zero or negative slope, it is interesting to see what will give a lower slope. Negative slopes were found in some of the measurements. An increase in σ_y^{MDc}, m, $\sigma_y^{MD/ZD}$ or G_{13} will generally cause a higher slope value, while an increase in ε_C, σ_y^{ZDt} or E_1, causes a lower one. See fig. 5.5.

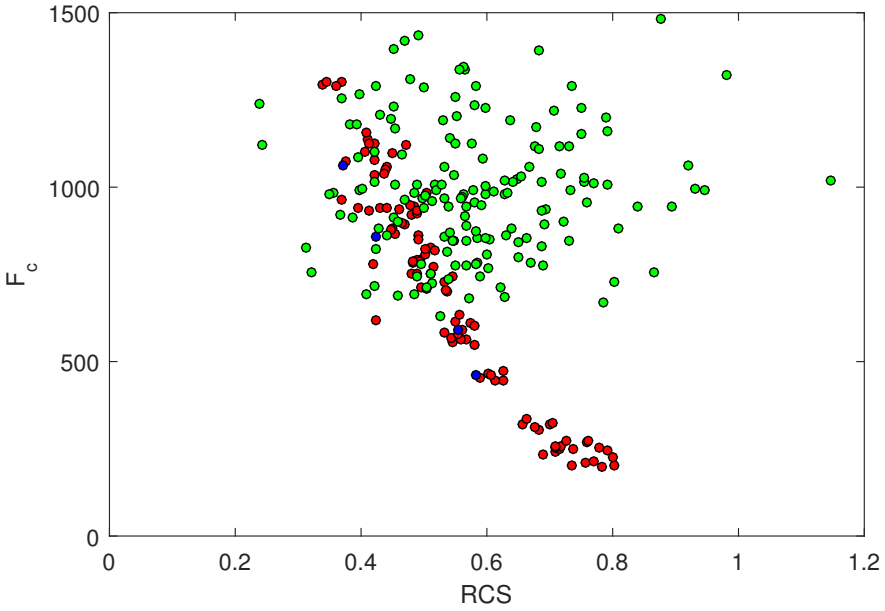

Figure 6.3: Scatter plot of RCS (horizontal axis) and F_c (vertical axis), combined from DOE results and fig. 1.10. Experimental data in red and earlier simulated data in blue, both of which examine the response subject to different male die widths, and different creasing depths. The experiments also include paperboard from different suppliers. Data from this DOE is in green, using varying materials but keeping everything else fixed.

In fig. 6.3, no correlation between RCS and creasing force with respect to varying material parameters can be found, although the material model correctly recreates this correlation when only considering different male die widths and creasing depths. It is concluded that the correlation is restricted to creasing geometries, unless there are interaction effects between the base material properties and creasing geometries – these were not tested in the DOE. Another observation is that the low F_c found in the reference data could not be recreated just by using different materials, which suggests that the crease depth and male die width must be varied as well, in order to recreate these low values.

The simulations generally overestimate the angle, when compared to experiments; the lowest measured angles in the simulations correspond to this value caught from experiments. The materials which come closer to experiments for response are those with lower ε_C, $\sigma_y^{MD/ZD}$, k and σ_y^{MDc}, and higher m, E_1, G_{13}, in accordance with the sign of their regression coefficients; see fig. 5.7.

6.3 Summary of factors

In this section, the influence of the parameters on the responses are summarised. The variables are classified by significance in table 6.1. The primary and second most important factors are displayed in table 6.2, based on the estimated regression coefficients.

Table 6.1: Summary of the coefficients' significance levels, as defined in section 2.3.3, utilising the ratio between an estimated regression coefficient and its margin of error, c/Δ.

	Insignificant factors	Significant factors	Very significant factors
$c/\Delta \in$	$[0, 1)$	$[1, 3)$	$[3, \infty)$
RCS	E_{3t}, G_{13}, ν_{12}, k, m	E_1, σ_y^{ZDt}, $\sigma_y^{MD/ZD}$	σ_y^{MDt}, σ_y^{MDc}, ε_C
$F_{f,C}$	E_{3t}, ε_C	E_1, G_{13}, ν_{12}, σ_y^{ZDt}, k, m	σ_y^{MDt}, σ_y^{MDc}, $\sigma_y^{MD/ZD}$
$F_{f,U}$	E_1, E_{3t}, ν_{12}, σ_y^{ZDt}	G_{13}, σ_y^{MDt}, $\sigma_y^{MD/ZD}$, m	σ_y^{MDc}, ε_C, k
F_c	E_{3t}, σ_y^{MDc}, σ_y^{ZDt}, $\sigma_y^{MD/ZD}$	G_{13}, m	E_1, ν_{12}, σ_y^{MDt}, ε_C, k
s_f	E_{3t}, ν_{12}, σ_y^{MDt}, k	G_{13}, $\sigma_y^{MD/ZD}$	E_1, σ_y^{MDc}, σ_y^{ZDt}, ε_C, m
s_c	E_{3t}, σ_y^{MDc}, σ_y^{ZDt}	G_{13}, ν_{12}	E_1, σ_y^{MDt}, $\sigma_y^{MD/ZD}$, ε_C, k, m
$\theta_{P,cm}$	E_{3t}, ν_{12}, σ_y^{ZDt}	E_1, G_{13}, σ_y^{MDt}, σ_y^{MDc}, k, m	$\sigma_y^{MD/ZD}$, ε_C

Table 6.2: Primary factors affecting the responses. The most and second most important factors for every response are marked by 1 and 2, respectively.

	RCS	$F_{f,C}$	$F_{f,U}$	F_c	s_f	s_c	$\theta_{P,cm}$
E_1						1	
σ_y^{MDt}	2	1					
σ_y^{MDc}	1		1	2	1		
$\sigma_y^{MD/ZD}$		2					2
ε_C			2	1	2	2	1

6.4 Linear vs quadratic model

The Q^2 of the quadratic models are significantly higher than those of the linear models (see figures 6.1–6.2). Additionally, predicted values come closer to observed values for the quadratic models (see figures A.2–A.3). This indicates that the quadratic model performs better in prediction, which is to be expected, as the quantities measured are assumed to be markedly nonlinear.

6.5 Direct vs indirect RCS model

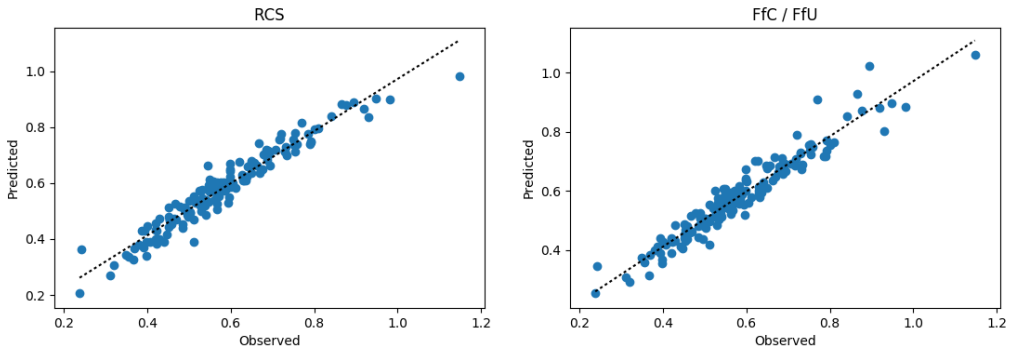

Figure 6.4: Comparison of predicted RCS values from the RCS regression model (left) and from the ratio between values from the creased and uncreased folding force regression models (right). Quadratic models are used here.

While a regression model has been posed for the RCS directly, it should also be possible to model it by considering the forces that define the RCS, an indirect model. R^2 was calculated to 0.933 for the direct model, and 0.926 for the indirect model. This, together with visual inspection of fig. 6.4, does not show any indication that one model should be superior to the other, results-wise.

If one of these models should be used for prediction values, the direct model is recommended, because of the fewer steps required.

7 Further work

The material model ignores effects related to humidity, temperature and rate-dependence. Also mentioned are some aspects that the model does not predict correctly, namely the pivoting angle and the folding slope. If a similar material model taking these effects into account were developed, or one that more accurately predicts these responses, it would be relevant to conduct a similar study with this new material model.

This work also does not examine the effects of geometrical factors such as paper thickness, die misalignment and crease depth, with the interaction of all the parameters.

The model also ignores the effects of damage, i.e. degradation of the elastic properties; it is currently in development to account for it. It may be relevant to investigate the effects of the plastic spin tensor in a DOE as well, for instance by including a parameter that scales it between 0 and 1. It also does not consider inhomogeneous materials, which often is the case for packaging materials, often made up of different types of paperboard.

It is of course also possible to include any other parameter present in the model. Not to mention additional output responses as needed, such as the shear stress in the paperboard during creasing, which is suspected to be correlated with the shape of the force curve during creasing, as mentioned in section 1.

8 References

[1] *Getting Started with Abaqus: Interactive Edition*. Dassault Systèmes, 2013.

[2] *Abaqus Scripting Reference Manual*. Dassault Systèmes, 2012.

[3] Baum, G. A., Brennan, D. C., Haberger, C. C., *Orthotropic elastic constants of paper*. Tappi Journal, 1981.

[4] Borgqvist, E. et al., *Continuum modelling of the mechanical response of paper-based materials*. Lund University, 2016.

[5] Eriksson, L., et al., *Design of Experiments: Principles and Applications*, third edition. Umetrics Academy, 2008.

[6] Gavelin, G., Borg, O.F., *Papperstillverkning*. Sveriges skogsindustriförbund, 1986.

[7] Krenk, S., *Non-linear Modeling and Analysis of Solids and Structures*. Cambridge University Press, 2009.

[8] Lindström, T., *In-plane paperboard model*. Lund University, 2013.

[9] Nygårds, M., Just, M., Tryding, J., *Experimental and numerical studies of creasing of paperboard*. Elsevier Ltd., 2009.

[10] Ottosen, N. S., Ristinmaa, M., *The Mechanics of Constitutive Modeling*. Elsevier Ltd, 2005.

[11] Santner, T. J., Williams, B. J., Notz, W. I., *Space-Filling Designs for Computer Experiments*. Springer Science+Business Media New York, 2003.

[12] Tayeh, R., *Determination of the out-of-plane shear properties of paperboard*. Lund University, 2015.

[13] Xia, Q. S., Boyce, M. C., *A constitutive model for the anisotropic elastic–plastic deformation of paper and paperboard*. Elsevier Ltd., 2002.

A Appendix

A.1 Experimental folding curve

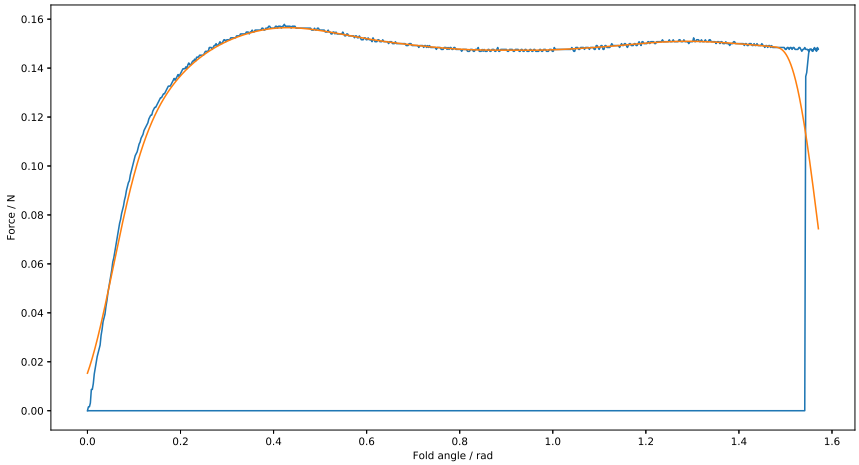

Figure A.1: Experimental data: force curve for folding a creased sample (blue) and the same curve after smoothing (orange). The experimental curve was obtained using a similar method as in [4, p. 10].

A.2 Trial design matrix

```
-0.469 0.429 -0.02 -0.755 -0.755 -0.918 -0.429 -0.388 0.633 -0.878 0.02
-0.714 -0.959 0.755 0.061 0.265 0.469 0.551 0.878 -0.306 -0.633 0.061
-0.02 0.714 0.673 0.673 -0.265 -0.633 -0.102 -0.918 0.878 0.673 -0.224
0.265 1.0 -0.224 0.918 0.469 0.184 -0.306 0.347 -0.429 0.796 -0.837
0.224 0.51 -0.469 -0.633 -0.469 0.388 0.184 -0.469 0.918 0.633 1.0
-0.347 -0.429 -0.755 -0.51 0.837 0.755 -0.061 -0.592 0.265 -1.0 -0.184
0.551 0.633 0.061 -0.061 0.061 0.959 0.959 0.061 -0.673 -0.714 -0.551
-0.755 -0.878 -0.51 -0.469 0.184 -0.796 0.796 -0.429 0.347 0.388 0.061
-0.184 -0.02 1.0 -0.837 -0.429 0.306 0.837 -0.02 0.959 0.143 -0.469
0.633 0.224 -0.388 0.837 0.796 0.061 -0.714 -0.102 0.551 -0.388 0.878
0.469 0.184 -0.837 0.592 -0.306 -0.673 -0.388 -1.0 -0.265 -0.51 -0.755
-0.102 0.061 -0.265 -0.918 0.878 0.429 -0.224 0.918 0.51 0.551 -0.714
0.878 0.306 -0.551 0.143 0.633 -0.184 0.918 -0.224 1.0 0.061 -0.592
0.918 -0.837 0.184 -0.796 0.551 0.837 0.469 -0.184 -0.143 0.469 0.51
0.061 -1.0 0.265 0.347 -0.959 0.347 -0.551 -0.837 0.755 -0.143 0.143
-0.429 -0.755 -0.184 0.796 0.388 -0.388 -0.469 0.429 0.837 -0.347 -0.918
-0.878 -0.102 0.347 -0.673 -0.714 0.592 0.224 -0.878 -0.755 -0.224 0.265
0.714 -0.918 -0.061 -0.878 -0.51 -0.061 -0.02 0.306 -0.061 -0.755 -0.878
-0.633 -0.224 0.061 0.959 0.51 1.0 0.51 -0.51 0.388 0.51 0.184
0.02 -0.265 0.02 0.878 -0.224 0.878 -0.918 0.061 -0.796 -0.837 -0.265
0.184 -0.061 0.878 0.429 0.918 -0.592 0.673 0.469 0.061 0.959 0.429
0.306 0.347 -0.143 -0.959 0.592 -0.306 0.592 0.796 0.184 -0.796 0.755
-0.306 0.959 -0.959 0.265 0.347 -0.143 0.633 -0.633 -0.633 -0.184 0.714
0.347 -0.633 0.51 -0.388 -1.0 -0.755 0.306 0.551 -0.102 0.224 0.959
-0.51 -0.51 0.918 -0.592 0.714 -0.224 -0.755 -0.061 0.796 -0.061 0.673
0.837 0.143 0.306 0.714 -0.551 0.224 0.061 -0.673 -0.878 0.714 0.551
-0.224 0.551 0.469 -0.265 0.959 0.673 -0.51 0.388 -1.0 0.184 0.633
-0.918 0.878 0.551 0.061 1.0 -0.347 0.347 -0.143 0.224 -0.551 -0.51
0.796 0.592 0.592 -0.551 0.061 0.633 -0.878 -0.755 0.306 -0.265 -0.388
-0.061 -0.714 0.633 0.02 0.755 -0.02 -0.184 -0.714 -0.714 0.347 -1.0
0.592 -0.673 -0.878 0.551 0.673 -0.265 0.429 0.633 -0.837 0.02 -0.02
1.0 -0.592 -0.306 -0.102 0.02 -0.714 -0.796 0.02 0.469 1.0 -0.143
-0.265 0.918 0.959 0.469 -0.592 0.265 0.143 0.265 0.143 -0.592 0.918
-0.959 -0.347 0.224 1.0 -0.061 -0.878 -0.347 -0.265 -0.551 -0.02 0.592
-0.837 0.388 -0.633 -0.306 0.429 -0.102 -1.0 -0.796 -0.02 0.837 -0.061
-0.592 -0.796 -0.796 -0.02 -0.143 0.551 -0.673 0.755 0.061 0.306 0.837
0.143 -0.469 -1.0 -0.143 -0.673 0.714 0.265 -0.347 -0.224 0.878 -0.796
0.51 -0.388 0.714 0.224 0.306 -0.469 0.714 -0.959 0.02 -0.918 0.388
-0.143 -0.143 0.388 0.755 -0.918 -0.551 0.878 0.184 -0.347 0.061 -0.959
0.755 0.796 -0.714 -0.347 -0.878 0.143 -0.633 0.673 -0.51 -0.102 0.224
-0.796 0.837 -0.429 0.184 -0.633 0.918 -0.265 0.143 0.714 -0.306 -0.633
```

0.061 −0.306 −0.918 0.51 −0.837 0.061 0.755 0.224 0.429 −0.959 0.469
0.959 −0.184 0.429 0.633 −0.347 0.796 0.061 1.0 0.592 0.265 −0.102
0.388 −0.551 −0.347 −0.714 0.143 −0.51 −0.837 −0.551 −0.918 −0.429 0.796
−0.673 0.469 −0.102 −0.224 −0.388 0.51 1.0 0.837 −0.469 0.918 0.347
0.429 0.755 0.143 −1.0 −0.02 −0.837 0.388 −0.306 −0.592 0.592 −0.347
−1.0 0.061 −0.673 −0.429 −0.102 −0.429 −0.143 0.592 −0.959 −0.469 −0.673
−0.388 0.673 −0.592 0.388 −0.184 −1.0 0.02 0.959 0.673 0.429 0.306
−0.551 0.02 0.837 −0.184 −0.796 0.02 −0.959 0.51 −0.184 0.755 −0.429
0.673 0.265 0.796 0.306 0.224 −0.959 −0.592 0.714 −0.388 −0.673 −0.306
−0.7293 −0.4336 0.3684 −0.6842 0.7694 −0.1679 −0.4982 −0.8847 −0.3935 −0.7544 0.0075
−0.8496 −0.5639 0.5138 −0.7995 0.3835 0.5338 0.1004 −0.6742 0.4687 0.5038 −0.599
0.1679 −0.5388 −0.0627 0.6491 −0.8145 −0.5639 −0.8803 0.6591 −0.9449 0.0075 −0.0376
−0.8095 0.619 0.0376 0.5188 0.8647 0.609 −0.7974 0.5439 0.4286 0.3083 −0.3383
0.6892 −0.2381 0.6642 0.1629 0.4085 0.4035 −0.6685 0.2732 0.9148 0.9449 0.3835
0.5038 0.5739 −0.213 −0.1278 −0.7995 0.9098 −0.6823 −0.4035 0.4236 −0.6491 0.6692
0.6391 −1.0 0.9048 0.4135 −0.4286 −0.4236 −0.0746 0.1078 −0.5539 −0.7594 0.2982
0.5338 −0.1028 −0.8797 −0.589 −0.4987 0.5639 0.1786 −0.8947 0.2581 −0.7644 −0.4837
0.4185 0.8546 0.6942 0.0627 −0.995 0.0376 −0.4705 −0.2381 −0.3383 −0.8246 −0.3985
0.8647 0.6391 0.7193 −0.2531 0.0526 0.0977 0.6298 −0.6642 0.7845 −0.0627 0.589
0.1078 −0.188 0.9248 −0.619 0.4486 −0.619 0.3674 −1.0 −0.3534 0.3885 0.4286
0.6742 0.5288 0.1378 −0.9048 −0.5739 −0.3484 0.8232 −0.0125 0.2381 −0.4987 −0.6541
0.4937 −0.7544 −0.6391 −0.0727 −0.9148 −0.193 −0.4383 0.0075 0.6792 −0.1178 0.9549
−0.0476 0.8847 0.7093 0.0727 0.9298 −0.1529 −0.4567 −0.5689 0.9048 0.0526 0.3484
0.3484 0.7544 −0.3684 0.3283 0.9449 −0.8045 −0.8527 0.3835 0.5539 −0.1429 −0.4185
−0.3734 0.6441 −0.2231 −0.9649 0.0827 0.9749 −0.3554 0.7393 0.1378 −0.0075 0.5789
−0.8045 0.3233 0.7143 0.7444 −0.3734 0.8697 −0.1022 0.7343 −0.1028 0.5288 0.4185
0.4436 0.1078 0.8697 −0.8647 −0.1378 0.6942 0.1878 0.7494 −0.4135 −0.2632 −0.7794
0.5589 −0.3584 −0.5188 −0.7093 0.1579 −0.4336 0.6252 0.4787 0.0125 0.7494 −0.9449
−0.3885 −0.8045 −0.6441 0.7895 −0.5188 −0.589 0.0773 0.594 −0.3484 0.4085 0.8997
0.8195 −0.3634 0.985 −0.3885 −0.1178 −0.9248 0.1694 −0.0175 −0.3784 0.0627 −0.8095
0.213 −0.0977 −0.9148 0.6792 0.0276 0.5088 0.0497 −0.9348 0.3333 −0.0476 0.9649
−0.1178 −0.6491 0.4286 −0.1679 −0.0927 −0.6291 0.6713 0.7895 0.4386 −0.599 −0.9398
−0.99 0.9549 −0.5388 −0.4737 0.7845 −0.0025 −0.4521 −0.208 −0.1479 −0.5288 0.2281
−0.9699 0.7143 0.6892 −0.5038 −0.0075 0.2832 0.5055 −0.0827 0.5489 0.6441 0.5088
−0.584 0.3835 0.7995 0.5439 0.7444 −0.0476 −0.9171 0.213 −0.619 −0.6792 −0.0777
0.0977 −0.1429 −0.0927 0.4687 −0.9549 −0.8947 −0.0654 −0.8446 −0.7243 −0.3985 0.5489
−1.0 0.1378 −0.0125 0.3434 −0.0226 0.8195 −0.7928 −0.1228 0.198 −0.7694 0.7444
−0.5238 0.2431 −0.3233 −0.7895 0.4436 −0.8647 −0.2219 −0.7895 0.7544 0.193 0.6792
−0.0025 0.3033 0.3033 −0.8596 −0.7895 −0.5188 −0.6041 0.2632 0.8697 0.7945 0.3333
−0.5489 −0.3835 −0.9398 0.8195 0.1028 −0.1629 −0.0378 −0.7193 −0.9348 0.3233 0.1579
−0.3484 0.6491 0.3885 −0.99 0.0175 0.4637 0.0359 −0.7845 0.5739 −0.8747 0.3634
−0.7995 −0.7845 0.609 0.594 −0.9098 −0.604 0.0681 0.0175 0.4085 −0.6992 0.0877
0.1178 0.0476 0.7945 0.9749 0.7794 −0.0677 −0.8573 −0.3885 0.0075 0.6591 −0.4937
−0.5539 −0.2632 0.0927 −0.203 −0.7744 0.4236 0.6943 −0.995 0.8346 −0.0927 0.0727
0.6241 0.0426 0.3734 0.2231 −0.589 0.8246 0.2845 0.1629 0.5639 −0.9048 −0.8496
−0.9198 −0.5739 −0.4185 −0.0777 0.3534 −0.8596 −0.1713 0.8747 −0.4035 0.8145 −0.1729
−0.0727 −0.8296 −0.0025 0.609 −0.1078 0.8396 0.6436 0.3885 −0.9398 0.1028 0.5138
−0.4135 −0.599 0.604 0.6391 −0.7945 −0.0326 −0.0792 0.1378 0.9449 0.8446 0.5288
0.594 −0.7093 −0.3133 0.8145 0.3885 0.7043 −0.1252 −0.7594 0.5038 −0.3383 −0.7694
0.188 0.8647 −0.4085 0.2782 0.7093 −0.4737 −0.5166 −0.3333 −1.0 −0.5789 −0.594
−0.2431 0.1729 0.4787 0.8596 −0.6391 0.2732 −0.9494 0.4687 0.5589 −0.4637 −0.5439
−0.4787 0.1679 0.9549 0.9499 0.1779 −0.8697 −0.0055 0.5739 0.1629 −0.1028 −0.6842
0.1278 0.8246 0.5238 0.1328 −0.1679 −1.0 0.3167 0.0276 0.3935 0.7594 0.7945
0.9098 −0.4937 −0.9449 −0.5739 0.3784 −0.5088 0.0129 −0.604 0.7895 0.0927 0.2331
−0.4937 0.2832 0.218 0.6842 0.8596 −0.3935 0.6574 −0.9599 −0.6491 −0.1529 −0.1378
−0.2281 0.6742 −0.7093 0.3534 −0.1128 −0.0426 0.7449 0.6441 0.2932 −0.7393 −0.9048
0.7093 0.0376 −0.8195 −0.3634 0.4386 0.4135 −0.4659 −0.3684 −0.7393 0.3985 −0.9749
0.1729 0.4135 0.9499 −0.6642 −0.0576 0.0075 −0.2542 0.5539 −0.4085 0.8697 0.9298
−0.4887 −0.9298 0.4937 −0.2932 −0.5789 −0.6992 0.1464 −0.9799 −0.198 0.1779 −0.6391
0.6642 −0.9348 −0.5539 0.4386 −0.193 −0.198 0.5654 −0.2982 0.193 0.9549 0.3885
0.1228 −0.1178 0.5539 0.9649 −0.1779 −0.4937 −0.3462 −0.6842 −0.9549 −0.2231 −0.7945
0.1128 −0.1629 0.3383 −0.4486 0.1328 1.0 −0.9862 −0.0977 0.1128 0.6942 −0.8045
0.3835 −0.9649 0.9398 −0.9699 −0.0426 0.0226 −0.5074 0.3283 0.4135 0.1629 −0.198
−0.3383 0.3383 −0.9749 0.1479 0.9549 −0.3033 0.2707 −0.1378 −0.2932 0.99 −0.4386
0.0376 0.9198 0.8496 0.6591 −0.4085 −0.4286 −0.2956 0.5338 −0.9799 0.2632 0.1278
0.6992 −0.7293 0.0326 −0.1228 0.995 −0.5138 −0.8204 −0.4536 0.1529 −0.1378 −0.6291
−0.3233 0.0125 0.995 −0.5439 −0.7293 0.9348 −0.4613 −0.198 0.7043 0.1128 0.3083
−0.8747 0.0226 0.3233 0.9248 0.3133 0.6241 0.57 0.2882 −0.5689 −0.213 −0.7293
−0.2832 0.9799 0.99 0.2331 0.0877 0.5138 −0.2357 0.1028 −0.2832 0.2531 −0.995
0.4987 0.7794 −0.7494 0.5088 −0.2231 −0.584 0.0543 0.4887 −0.6341 0.8997 0.3584
−0.0226 0.6692 −0.6291 0.995 −0.6491 0.0627 −0.977 −0.1479 −0.4486 −0.2431 0.4386
−0.0576 1.0 0.208 −0.4286 0.1679 −0.3734 −0.4153 −0.9098 −0.614 0.0326 0.9599
−0.9398 −0.3183 −0.4637 −0.1579 0.0025 −0.4787 0.5331 −0.5489 0.3784 −0.985 −0.5639
0.0175 0.3885 0.1078 −0.7694 0.7243 0.8145 0.0451 −0.9649 0.203 0.7343 0.4987
−0.7494 −0.2782 −0.1729 −0.0276 −0.4336 −0.2832 −0.1667 0.4536 −0.9499 −0.8396 0.8446
0.5138 0.4687 −0.8346 −0.3684 0.4637 0.7945 0.197 0.0426 0.9649 −0.4236 0.5589
0.4386 −0.6541 0.2932 −0.4937 0.4586 0.1078 −0.825 0.7744 −0.7043 −0.8195 0.4236
0.218 −0.584 0.1429 −0.8496 0.3434 −0.2732 0.3029 0.203 0.7293 0.8747 0.9499
0.8396 −0.2531 0.4687 −0.584 −0.3434 0.1429 −0.6317 −0.9549 0.0777 0.604 0.7995
−0.9449 0.7995 0.0476 0.7043 −0.3784 −0.3584 −0.07 −0.2281 −0.3734 −0.9649 −0.2531
0.2481 0.9148 −0.0877 −0.0827 0.8496 0.5038 0.4457 0.604 0.2481 0.8396 0.4135
−0.9248 −0.5439 −0.4486 −0.1629 −0.8697 −0.0977 0.593 0.3534 0.1779 0.3534 −0.7744

−0.5439 0.1579 −0.8446 0.5338 0.1479 0.99 0.2891 0.9599 0.1078 0.4536 −0.3133
−0.4737 −0.3784 −0.6792 −0.5489 −0.7544 0.995 0.2799 0.6391 −0.4787 −0.4135 0.0627
0.6942 0.2481 0.6591 −0.8847 −0.594 0.3383 0.1096 0.4737 0.3885 −0.8496 0.7243
−0.203 −0.6842 −0.3333 0.5639 0.8797 0.208 −0.7744 0.4637 −0.7794 0.4787 −0.6491
−0.8246 0.985 −0.0677 0.8697 0.1128 −0.1178 −0.2127 −0.6241 −0.1078 0.7895 −0.0025
−0.7744 0.8496 0.8647 −0.6992 −0.2531 0.2381 −0.36 0.2531 −0.6742 −0.589 0.3985
−0.2732 −0.8697 −0.1378 0.5789 −0.8446 0.4286 0.4272 −0.7043 −0.5138 −0.609 −0.3183
−0.8596 0.5439 −0.3083 0.3083 0.5288 0.1378 0.5884 −0.594 0.7794 −0.6241 0.7043
0.2281 −0.2281 −0.9298 0.0326 −0.9749 −0.5589 −0.0608 −0.584 0.6692 0.4637 −0.6341
−0.4436 0.1479 −0.9599 0.3033 −0.4386 −0.1028 −0.7652 0.6241 0.0226 0.4286 −0.985
0.2732 0.8396 0.2682 0.619 0.2632 0.3784 −0.0332 −0.99 −0.183 −0.9599 0.4486
0.619 −0.7043 0.8747 0.3133 −0.9348 0.8647 −0.2403 −0.0727 −0.3283 0.2431 −0.3534
−0.0426 −0.5038 −0.2882 0.5539 −0.1228 −0.9398 0.4318 −0.6692 0.8446 −0.4035 0.6942
−0.9148 0.9398 −0.0827 −0.5539 −0.0727 0.1729 −0.291 0.5789 −0.4185 0.9298 −0.4286
0.5288 0.5489 −0.7945 0.6992 −0.203 −0.2632 −0.2634 −0.3383 0.99 −0.8947 0.0276
−0.5288 −0.6241 −0.3484 −0.609 0.2982 0.7895 0.2016 0.5138 −0.6391 0.9248 −0.5589
−0.8647 0.4887 −0.614 0.5038 −0.9499 0.1028 0.2753 0.3033 −0.9148 0.2581 0.0226
−0.1429 0.0927 −0.5789 0.3634 −0.5338 −0.6591 −0.6179 −0.599 0.1278 0.9348 0.9098
−0.0526 0.599 0.213 0.985 0.5188 0.0927 0.3766 0.5188 −0.7444 −0.4336 0.9048
0.8997 0.9248 0.1328 −0.9348 −0.4436 0.6892 0.2155 −0.1429 −0.2982 0.4837 0.2882
0.6692 0.2732 −0.9348 0.2832 −0.4737 0.7093 0.8048 0.3484 −0.1579 0.3133 0.619
0.4637 −0.0276 −0.5489 0.7243 0.4135 0.193 −0.5672 0.6942 −0.0877 −0.9449 −0.9348
0.8847 0.2531 0.4336 −0.9148 0.589 −0.3434 −0.1483 −0.4386 0.604 0.8496 −0.3484
0.3684 0.183 −0.985 −0.5789 0.188 0.2481 −0.1437 −0.3033 −0.6291 0.8546 0.9348
0.6341 −0.1679 0.8797 0.1529 0.604 −0.208 −0.7882 −0.7093 −0.7293 −0.3835 0.5739
0.4336 −0.1529 0.8396 −0.5338 0.7143 0.9699 0.2109 0.1679 0.9348 −0.2882 0.1028
−0.0827 0.7193 −0.9198 −0.7293 −0.198 0.2632 0.7357 −0.0777 −0.7694 0.3584 −0.3784
−0.2331 −0.6692 0.4837 0.0677 −0.1479 −0.7845 −0.9263 −0.0877 −0.0376 −0.9198 −0.7895
0.9198 0.0025 0.2431 0.0025 −0.0476 0.599 0.1832 0.6341 −0.8747 1.0 −0.213
−0.2531 −0.5138 0.3434 0.99 0.4737 −0.2782 −0.6869 0.9699 0.4937 0.0125 0.4637
0.985 −0.7243 −0.7243 −0.198 0.2732 0.6992 −0.7376 −0.4737 −0.1729 −0.4286 0.3534
0.0727 −0.6792 −0.218 0.3784 0.4837 0.8897 0.3306 0.7143 0.6742 0.3434 0.8797
0.0877 0.2782 0.5639 −0.9298 0.6692 −0.9799 −0.8619 0.1328 −0.1679 −0.0276 0.183
−0.1028 0.9699 −1.0 0.0175 0.1278 0.9248 −0.5258 −0.5589 0.0627 0.2331 −0.1278
0.6591 −0.8546 0.2982 −0.7193 0.0727 0.1679 0.7311 −0.8346 0.4486 −0.0677 −0.5739
−0.5038 0.4386 −0.7193 0.9048 0.9398 0.0125 −0.0239 −0.4236 0.3634 −0.4085 −0.7243
−0.594 −0.4987 −0.604 0.3584 −0.8246 0.8997 0.2201 −0.2431 0.0927 0.8246 0.5238
0.1028 −0.7744 0.6241 0.4787 0.2481 0.6591 −0.8343 0.3784 −0.6441 0.5138 0.7093

A.3 Observed vs predicted data

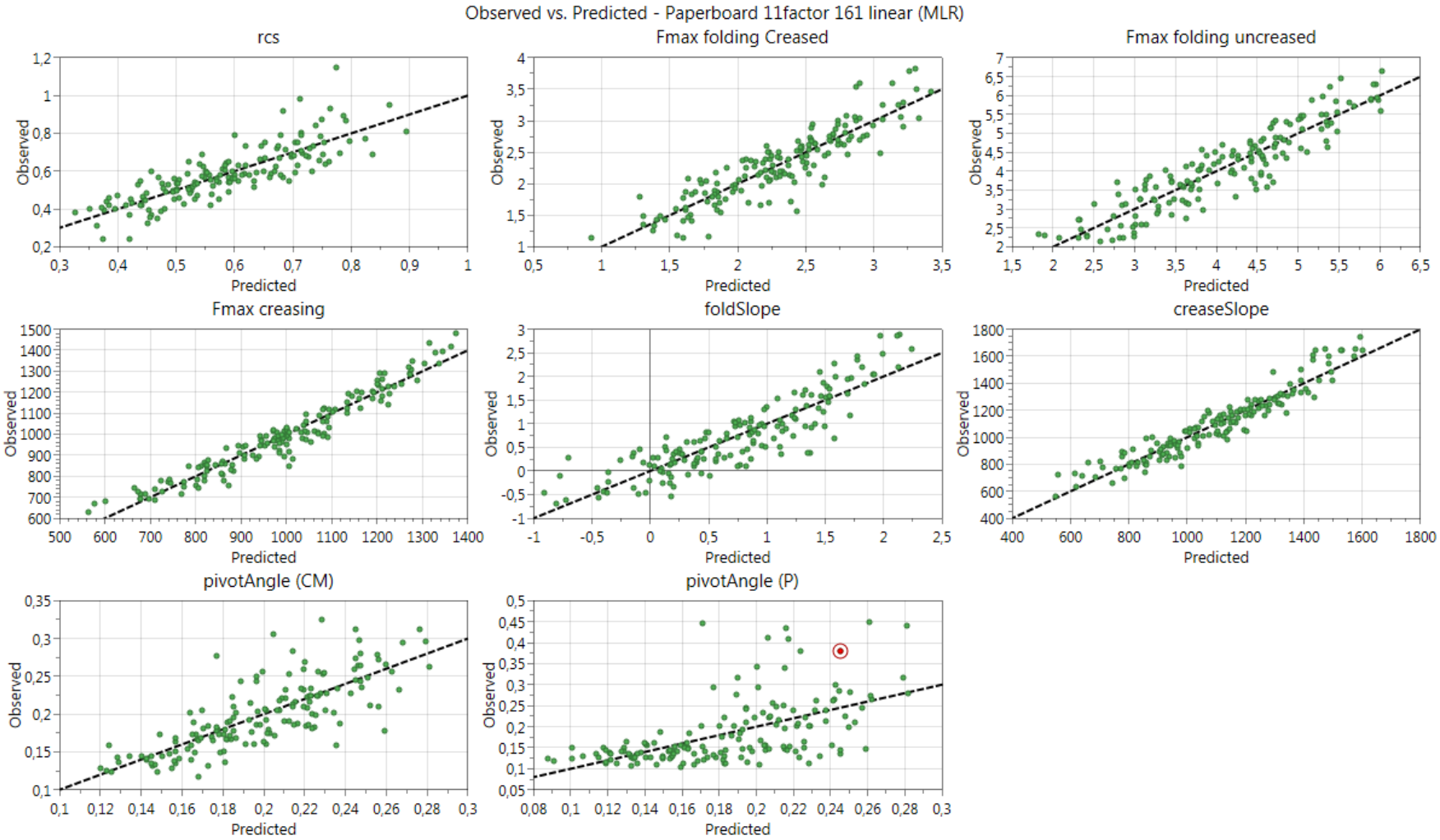

Figure A.2: Observed–predicted plots for the linear models.

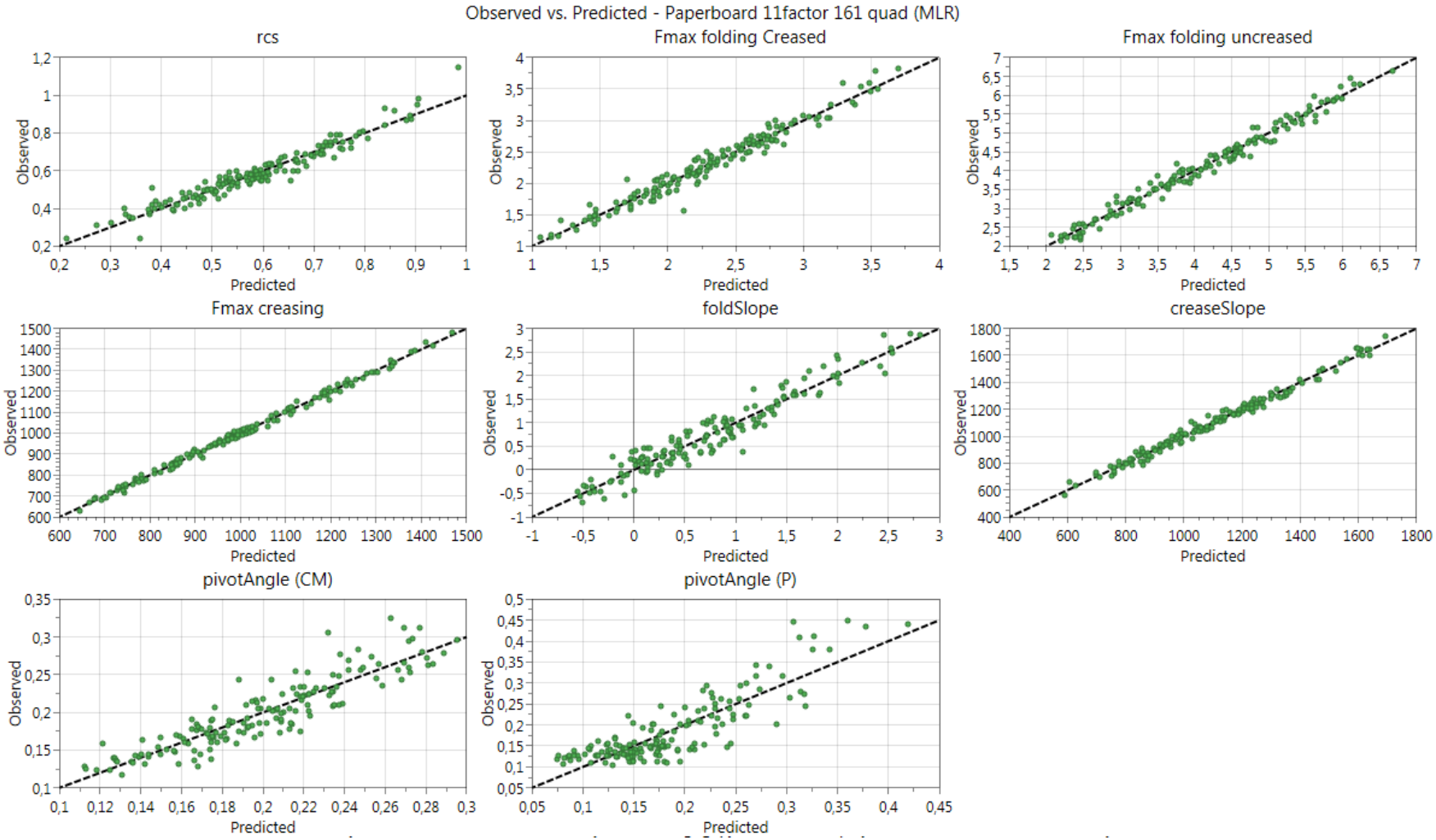

Figure A.3: Observed–predicted plots for the quadratic models.

A.4 Coefficients and confidence intervals of linear models

Table A.1: Estimated coefficient values, with their 95% confidence intervals.

	RCS	$F_{f,C}$/N	$F_{f,U}$/N	F_c/N	s_f/N	s_c/N	$\theta_{P,cm}$	$\theta_{P,p}$
Constant	0.574 ± 0.014	2.295 ± 0.043	4.136 ± 0.073	989.534 ± 8.059	0.739 ± 0.062	1094.550 ± 12.910	0.201 ± 0.005	0.185 ± 0.011
E_1	-0.053 ± 0.024	-0.198 ± 0.076	0.019 ± 0.128	111.627 ± 14.127	-0.413 ± 0.109	251.321 ± 22.629	-0.014 ± 0.009	-0.019 ± 0.019
E_{3t}	-0.016 ± 0.023	0.007 ± 0.072	0.106 ± 0.122	0.060 ± 13.421	0.073 ± 0.104	0.927 ± 21.498	-0.007 ± 0.008	-0.008 ± 0.018
G_{13}	0.022 ± 0.022	0.208 ± 0.070	0.225 ± 0.119	29.079 ± 13.162	0.112 ± 0.102	-30.591 ± 21.083	-0.010 ± 0.008	0.002 ± 0.018
ν_{12}	0.008 ± 0.025	0.081 ± 0.079	0.117 ± 0.134	46.359 ± 14.827	-0.021 ± 0.115	32.602 ± 23.750	0.007 ± 0.009	0.008 ± 0.020
σ_y^{MDt}	0.111 ± 0.025	0.604 ± 0.077	0.286 ± 0.131	187.844 ± 14.420	0.080 ± 0.112	88.635 ± 23.099	0.023 ± 0.009	0.031 ± 0.019
σ_y^{MDc}	-0.138 ± 0.024	0.289 ± 0.074	1.347 ± 0.125	0.771 ± 13.811	0.648 ± 0.107	2.303 ± 22.122	0.011 ± 0.008	0.005 ± 0.018
σ_y^{ZDt}	-0.044 ± 0.026	-0.203 ± 0.081	-0.080 ± 0.136	3.518 ± 15.056	-0.491 ± 0.117	9.429 ± 24.117	0.006 ± 0.009	0.001 ± 0.020
$\sigma_y^{MD/ZD}$	0.070 ± 0.024	0.361 ± 0.075	0.155 ± 0.127	-0.062 ± 14.034	0.253 ± 0.109	107.278 ± 22.481	0.027 ± 0.009	0.029 ± 0.019
ε_C	0.078 ± 0.024	-0.057 ± 0.075	-0.737 ± 0.126	-215.349 ± 13.954	-0.508 ± 0.108	-211.431 ± 22.352	0.042 ± 0.009	0.058 ± 0.019
k	-0.019 ± 0.021	0.137 ± 0.066	0.384 ± 0.111	60.876 ± 12.280	0.082 ± 0.095	74.761 ± 19.670	0.019 ± 0.008	0.020 ± 0.016
m	-0.013 ± 0.023	0.119 ± 0.072	0.344 ± 0.121	23.137 ± 13.363	0.446 ± 0.104	198.089 ± 21.406	-0.016 ± 0.008	-0.015 ± 0.018

A.5 Pivoting angle scatter plot

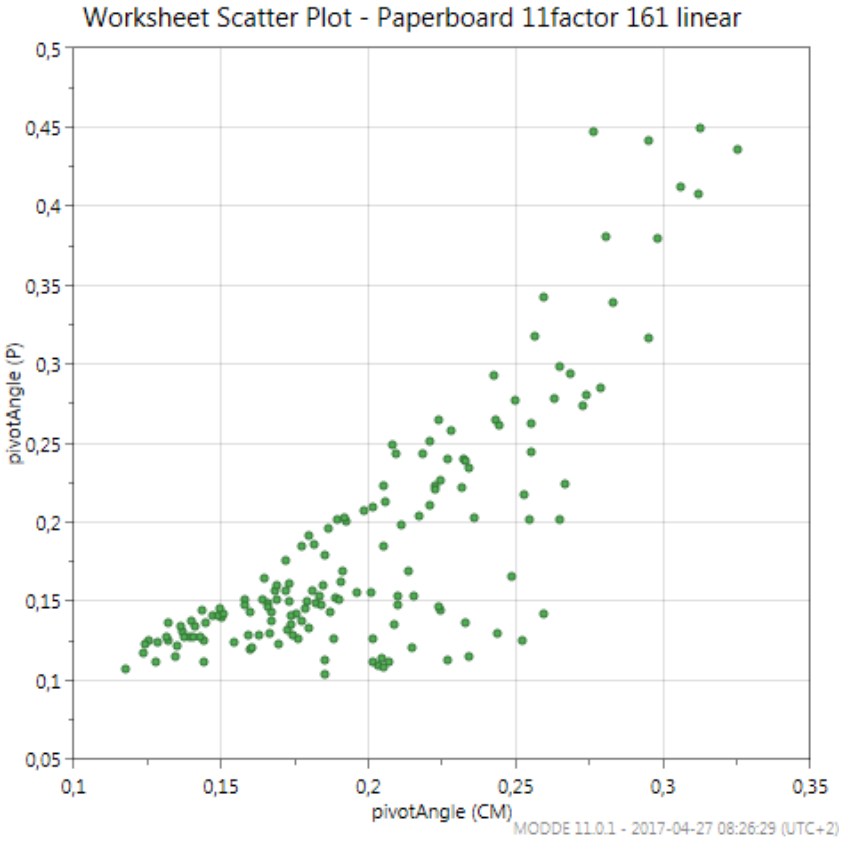

Figure A.4: Scatter plot of $\theta_{P,cm}$ (horizontal axis) and $\theta_{P,p}$ (vertical axis).

A.6 Coefficient data and related statistics of linear models

```
rcs Coeff. SC Std. Err. P Conf. int(±)
Constant 0,574068 0,00696985 0 0,0137757
E1 -0,053246 0,0122168 2,46726e-005 0,0241462
E3 -0,0157718 0,0116066 0,176296 0,0229401
G13 0,0219185 0,0113824 0,0561051 0,0224969
nu12 0,00755026 0,0128224 0,556887 0,0253432
sigmaMDt 0,111157 0,0124707 1,92276e-015 0,024648
sigmaMDc -0,138369 0,0119436 2,21185e-022 0,0236062
sigmaZDt -0,0440385 0,0130206 0,000924532 0,0257348
sigmaMD/ZD 0,0701428 0,0121369 4,4195e-008 0,0239883
epsilon_C 0,0783013 0,0120676 1,28341e-009 0,0238513
k -0,0192016 0,0106196 0,0726584 0,0209893
m -0,0125725 0,0115567 0,278445 0,0228415


N = 157 Q2 = 0,632 Cond. no. = 2,099
DF = 145 R2 = 0,686 RSD = 0,08509
R2 adj. = 0,662
Confidence = 0,95

Fmax folding Crea. Coeff. SC Std. Err. P Conf. int(±)
Constant 2,29458 0,0218334 0 0,043153
E1 -0,198318 0,0382698 7,22672e-007 0,0756391
E3 0,00723176 0,0363582 0,842605 0,071861
G13 0,207898 0,0356558 3,44549e-008 0,0704726
nu12 0,0805846 0,0401669 0,0466899 0,0793886
sigmaMDt 0,604427 0,0390651 1,67719e-032 0,0772109
sigmaMDc 0,289127 0,0374138 1,66469e-012 0,0739473
sigmaZDt -0,20298 0,0407876 1,81007e-006 0,0806155
sigmaMD/ZD 0,36064 0,0380195 6,6696e-017 0,0751445
epsilon_C -0,0569397 0,0378023 0,134174 0,0747152
k 0,136543 0,0332662 6,73433e-005 0,0657498
m 0,11904 0,0362019 0,00126526 0,071552


N = 157 Q2 = 0,762 Cond. no. = 2,099
DF = 145 R2 = 0,797 RSD = 0,2665
R2 adj. = 0,781
Confidence = 0,95

Fmax folding uncr. Coeff. SC Std. Err. P Conf. int(±)
Constant 4,13636 0,0369643 0 0,0730588
E1 0,0191012 0,0647914 0,768562 0,128058
E3 0,105984 0,0615551 0,0872434 0,121662
G13 0,224912 0,0603658 0,000278243 0,119311
nu12 0,11682 0,0680032 0,0879497 0,134406
sigmaMDt 0,285668 0,0661378 2,88806e-005 0,130719
sigmaMDc 1,34673 0,0633423 0 0,125194
sigmaZDt -0,0803241 0,0690541 0,246653 0,136483
sigmaMD/ZD 0,154579 0,0643677 0,0175948 0,127221
epsilon_C -0,737302 0,064 3,27731e-022 0,126494
k 0,384062 0,0563203 2,29455e-010 0,111316
m 0,344038 0,0612905 9,7875e-008 0,121139


N = 157 Q2 = 0,812 Cond. no. = 2,099
DF = 145 R2 = 0,840 RSD = 0,4513
R2 adj. = 0,827
Confidence = 0,95

Fmax creasing Coeff. SC Std. Err. P Conf. int(±)
Constant 989,534 4,07766 0 8,05937
E1 111,627 7,14737 7,15293e-033 14,1266
E3 0,0596828 6,79036 0,992975 13,4209
G13 29,0789 6,65916 2,38544e-005 13,1616
nu12 46,3593 7,50167 6,15273e-009 14,8268
sigmaMDt 187,844 7,29589 0 14,4201
sigmaMDc 0,770823 6,9875 0,912279 13,8106
sigmaZDt 3,5181 7,6176 0,644894 15,056
sigmaMD/ZD -0,0622354 7,10062 0,992975 14,0342
epsilon_C -215,349 7,06006 0 13,954
k 60,8758 6,21289 1,04253e-017 12,2796
m 23,1367 6,76116 0,000808013 13,3632


N = 157 Q2 = 0,922 Cond. no. = 2,099
DF = 145 R2 = 0,934 RSD = 49,78
R2 adj. = 0,929
Confidence = 0,95

foldSlope Coeff. SC Std. Err. P Conf. int(±)
Constant 0,738879 0,0316039 0 0,0624641
E1 -0,41312 0,0553957 7,402e-012 0,109488
E3 0,0733728 0,0526287 0,165396 0,104019
G13 0,112135 0,0516119 0,0314302 0,102009
nu12 -0,0209406 0,0581417 0,719252 0,114915
sigmaMDt 0,0798083 0,0565468 0,160273 0,111763
sigmaMDc 0,647591 0,0541567 2,31319e-023 0,107039
sigmaZDt -0,490881 0,0590402 6,09965e-014 0,116691
sigmaMD/ZD 0,253334 0,0550334 9,01034e-006 0,108772
epsilon_C -0,50811 0,054719 2,16949e-016 0,108151
k 0,0815564 0,048153 0,0924652 0,0951731
m 0,446093 0,0524024 1,95611e-014 0,103572


N = 157 Q2 = 0,738 Cond. no. = 2,099
DF = 145 R2 = 0,777 RSD = 0,3858
R2 adj. = 0,760
Confidence = 0,95

creaseSlope Coeff. SC Std. Err. P Conf. int(±)
Constant 1094,55 6,53178 0 12,9099
E1 251,321 11,449 0 22,6286
E3 0,927004 10,8771 0,932214 21,4983
G13 -30,5915 10,667 0,00474934 21,0829
nu12 32,602 12,0165 0,00747334 23,7503
sigmaMDt 88,6354 11,6869 3,68965e-012 23,0988
sigmaMDc 2,30333 11,1929 0,837253 22,1224
sigmaZDt 9,42945 12,2022 0,440914 24,1173
sigmaMD/ZD 107,278 11,3741 9,1717e-017 22,4806
epsilon_C -211,431 11,3091 0 22,3522
k 74,7612 9,9521 5,48818e-012 19,67
m 198,089 10,8303 0 21,4059


N = 157 Q2 = 0,887 Cond. no. = 2,099
DF = 145 R2 = 0,904 RSD = 79,74
R2 adj. = 0,897
Confidence = 0,95

pivotAngle (CM) Coeff. SC Std. Err. P Conf. int(±)
Constant 0,200715 0,0024854 0 0,00491262
E1 -0,0144993 0,00435107 0,00109453 0,00860029
E3 -0,00678982 0,00414878 0,103901 0,00820045
G13 -0,00983911 0,00404744 0,0162887 0,00800015
nu12 0,00732701 0,00458026 0,111858 0,00905331
sigmaMDt 0,0231784 0,00445018 6,46321e-007 0,00879619
sigmaMDc 0,0107378 0,004247 0,0125391 0,0083946
sigmaZDt 0,00578466 0,00465443 0,215952 0,00919992
sigmaMD/ZD 0,0272507 0,00435601 4,25744e-009 0,00861006
epsilon_C 0,0422886 0,00431144 1,03855e-017 0,00852196
k 0,0188641 0,00382062 2,16292e-006 0,00755181
m -0,01582 0,00412502 0,000187095 0,00815349


N = 156 Q2 = 0,547 Cond. no. = 2,114
DF = 144 R2 = 0,613 RSD = 0,03026
R2 adj. = 0,584
Confidence = 0,95

pivotAngle (P) Coeff. SC Std. Err. P Conf. int(±)
Constant 0,185291 0,00543127 0 0,0107347
E1 -0,0190911 0,00952 0,0467845 0,018816
E3 -0,00753454 0,00904448 0,406178 0,0178761
G13 0,00216379 0,00886973 0,807613 0,0175308
nu12 0,00765792 0,00999191 0,444675 0,0197487
sigmaMDt 0,0310238 0,00971782 0,00173016 0,019207
sigmaMDc 0,00485888 0,00930706 0,602416 0,0183951
sigmaZDt 0,000591535 0,0101463 0,953546 0,0200539
sigmaMD/ZD 0,0287583 0,00945774 0,00280154 0,0186929
epsilon_C 0,057962 0,00940371 6,67045e-009 0,0185862
k 0,0203749 0,00827531 0,0149833 0,0163559
m -0,0151881 0,00900559 0,0938405 0,0177993


N = 157 Q2 = 0,204 Cond. no. = 2,099
DF = 145 R2 = 0,322 RSD = 0,06631
R2 adj. = 0,270
Confidence = 0,95
```

A.7 Effects data of quadratic models

```
rcs Effect Conf. int(±)
σMDc*σMDc 0,307593 0,0505638
sigmaMDc -0,262212 0,0251914
sigmaMDt 0,244164 0,0257493
E1*σMDt 0,17328 0,0511475
epilson_C 0,132987 0,0256146
σMDt*σMDt -0,131309 0,0506647
σZDt*σZDt 0,121007 0,0537135
G13*σMDc -0,120551 0,043918
σZDt*σMDZD -0,113834 0,0509099
E1 -0,106383 0,0258851
sigmaMD/ZD 0,101166 0,0256242
σMDc*εC 0,0988595 0,0472719
sigmaZDt -0,0903112 0,028037
E1*E1 -0,0890251 0,0536216
σMDc*σZDt 0,0858532 0,0498581
σMDt*εC -0,0749718 0,0456905
E1*εC 0,0705573 0,0482924
E1*σMDZD 0,0676836 0,0481769
σMDZD*εC -0,0616795 0,0462789
k*m 0,0596986 0,0388479
m*m 0,0593298 0,0545509
k*k 0,0539587 0,037381
E1*σZDt 0,0529816 0,0484194
σMDc*k -0,05176 0,0416821
k -0,0458021 0,0221309
G13*σMDt 0,0450457 0,0430925
G13*εC -0,0434553 0,0430873
σMDc*m -0,0432755 0,0454271
ν12*σMDZD -0,0426141 0,0445763
G13 0,0408148 0,0234847
σMDt*σMDZD -0,0394482 0,0482961
E1*ν12 -0,0349805 0,0513838
m -0,0306305 0,023618
nu12 0,0159078 0,0269586
E3 -0,00566512 0,0240443

N = 157 Q2 = 0,883 Cond. no. = 8,955
DF = 121 R2 = 0,933 RSD = 0,04297
R2 adj. = 0,914
Confidence = 0,95

Fmax folding Creased Effect Conf. int(±)
sigmaMDt 1,23579 0,0838155
E1*σMDt 0,723727 0,158532
sigmaMD/ZD 0,711622 0,0799989
σZDt*σMDZD -0,55656 0,155775
sigmaMDc 0,52962 0,0769392
σMDt*εC -0,494868 0,140952
σMDt*σMDt -0,487775 0,163801
E1 -0,446727 0,0792164
G13 0,42645 0,0723988
σZDt*σZDt 0,405205 0,16904
sigmaZDt -0,361735 0,0861669
σMDc*σMDc -0,350791 0,155494
E1*εC 0,347846 0,147455
σMDt*σMDc 0,313604 0,151055
k 0,274129 0,0680467
E1*E1 -0,262723 0,16948
m 0,251588 0,0730501
σMDZD*εC -0,236861 0,142348
σMDc*m 0,234559 0,136249
E1*σMDc -0,22815 0,142572
σMDt*σZDt -0,207748 0,154492
m*m 0,206061 0,172011
σMDc*σMDZD 0,199391 0,132887
G13*σMDZD 0,180728 0,135599
σMDc*σZDt 0,179396 0,15289
G13*σMDt 0,172885 0,134052
E3*σMDc 0,163974 0,137302
σMDt*σMDZD 0,152624 0,149241
σMDZD*σMDZD -0,134342 0,16169
epilson_C -0,126152 0,078134
E1*σMDZD 0,120053 0,14857
k*k -0,11643 0,114836

foldSlope Effect Conf. int(±)
sigmaMDc 1,19553 0,145388
sigmaZDt -1,02153 0,154645
epilson_C -0,992821 0,149214
m 0,873885 0,137111
E1 -0,833247 0,143722
σMDc*m 0,825059 0,256256
σMDZD*εC -0,591685 0,267573
σMDc*σZDt -0,590289 0,2895
sigmaMD/ZD 0,56518 0,143314
σZDt*εC 0,521526 0,288681
σMDc*σMDc -0,521387 0,26365
σMDt*σMDc 0,462571 0,278852
σZDt*σMDZD -0,460359 0,287639
σZDt*m -0,438557 0,275151
σMDt*σZDt 0,403066 0,286683
k*m -0,382206 0,222618
σMDc*εC -0,366862 0,272577
σMDt*σMDZD -0,343893 0,27803
G13*k 0,321776 0,221493
σMDZD*m -0,302327 0,250482
G13*σMDZD 0,294782 0,242197
E1*εC 0,285263 0,265596
σMDc*k 0,275682 0,242268
k 0,256616 0,12603
σMDt*k 0,225482 0,239542
sigmaMDt 0,225144 0,155104
G13 0,207264 0,134692
E3 0,0601429 0,138257
nu12 0,00815943 0,153128

N = 157 Q2 = 0,875 Cond. no. = 4,884
DF = 127 R2 = 0,919 RSD = 0,2488
R2 adj. = 0,900
Confidence = 0,95

creaseSlope Effect Conf. int(±)
E1 488,748 19,109
epilson_C -388,394 19,3012
m 386,467 18,2607
sigmaMD/ZD 220,488 19,0057
εC*m -196,65 33,1338
sigmaMDt 180,209 19,5727
E1*σMDt 177,086 39,0286
σMDt*σMDt -161,697 39,0048
k 155,285 17,0491
εC*εC 145,955 38,0872
E1*εC -138,483 35,7828
k*k -137,595 27,5555
E1*E1 -100,672 38,7589
G13 -81,3798 17,9122
G13*m 71,7248 30,1374
k*m 53,0386 30,0206
G13*σMDZD -47,5311 32,7389
σMDt*εC -44,7619 34,5935
G13*εC -43,8336 32,3952
σMDt*m 42,0639 35,9525
σMDZD*εC 41,9648 35,579
ν12*m 41,6807 35,0956
σMDc*σMDZD -41,3237 33,618
nu12 40,2216 20,8597
εC*k -40,107 33,5429
σZDt*σMDZD 40,0898 37,6265
ν12*σMDZD 36,4271 35,0614
E3*σMDt 33,7528 35,3726
E1*k 30,4433 28,9466
E3*G13 29,7282 31,4977
ν12*k 28,9722 30,6205
ν12*σMDc 26,0459 36,2502
sigmaZDt -10,6932 20,9449
E3 5,6879 18,3272
sigmaMDc -3,64166 18,7013

N = 157 Q2 = 0,977 Cond. no. = 6,095
```

nu12 0,112325 0,0825929
G13*εC −0,100568 0,134516
E3 0,0871684 0,0751942

N = 157 Q2 = 0,925 Cond. no. = 10,51
DF = 121 R2 = 0,958 RSD = 0,1329
R2 adj. = 0,946
Confidence = 0,95

Fmax folding uncreased Effect Conf. int(±)
sigmaMDc 2,5903 0,0980302
σMDc*σMDc −1,80386 0,191642
epilson_C −1,43365 0,098078
σMDc*εC −1,16222 0,183999
σMDc*m 0,931099 0,177676
k 0,8247 0,0869605
m 0,706754 0,0939299
k*k −0,632248 0,148283
G13*σMDc 0,543321 0,170731
sigmaMD/ZD 0,531594 0,100164
sigmaMDt 0,50911 0,101305
σMDc*σMDZD 0,481412 0,173621
G13 0,429394 0,0925931
σMDZD*m −0,401042 0,171103
σMDc*k 0,342323 0,164944
εC*εC 0,337501 0,201948
σMDt*σMDc 0,294978 0,192962
E1*σMDt 0,281259 0,196444
G13*σMDZD 0,240375 0,169196
σMDZD*σMDZD −0,219106 0,199337
G13*εC 0,218442 0,170402
m*m −0,169277 0,1991
nu12 0,166644 0,104016
k*m −0,163751 0,151307
E3 0,087882 0,0950428
sigmaZDt −0,0763123 0,104874
E1 −0,031357 0,0988547

N = 157 Q2 = 0,969 Cond. no. = 7,914
DF = 129 R2 = 0,980 RSD = 0,1705
R2 adj. = 0,975
Confidence = 0,95

Fmax creasing Effect Conf. int(±)
epilson_C −424,567 8,40043
sigmaMDt 373,55 8,54205
E1 213,427 8,6721
E1*σMDt 155,971 16,8775
k 122,805 7,36095
E1*E1 −120,735 18,1531
k*k −118,246 12,5685
εC*εC 100,814 17,3692
σMDt*εC −83,7243 15,2413
nu12 72,6123 8,96289
σMDt*σMDt −64,0378 17,2232
G13*G13 −55,7526 15,985
G13 47,6457 7,92324
εC*k −41,2637 14,3533
m 39,5593 8,08732
m*m −38,7095 17,342
G13*εC −37,4835 14,3937
ν12*εC −25,5796 15,197
G13*m 24,3184 13,2935
E1*k 23,8508 12,9782
ν12*k 19,4184 13,7281
σZDt*σMDZD 18,5827 16,7133
σMDt*k 17,8835 14,0277
E1*σMDZD −17,1965 16,615
E1*ν12 16,2849 17,7064
σMDt*σMDZD −14,8937 16,4534
E3*εC −14,6381 14,7782
G13*σMDZD 13,9082 15,2926
ν12*m 13,7486 15,3567
E1*m −13,1501 15,8928
G13*k 12,562 12,9986
σMDZD*σMDZD −12,1333 18,0671
sigmaMD/ZD 11,2486 8,55322
E3 4,36366 8,13249
sigmaZDt −0,853973 9,15125
sigmaMDc −0,260193 8,13472

N = 157 Q2 = 0,992 Cond. no. = 10,17
DF = 121 R2 = 0,987 RSD = 32,65
R2 adj. = 0,983
Confidence = 0,95

pivotAngle (CM) Effect Conf. int(±)
σMDc*σMDc −0,0887323 0,027874
epilson_C 0,0808171 0,0132925
E1*E1 −0,0670045 0,0292246
σMDc*σZDt 0,0602879 0,0260536
sigmaMD/ZD 0,0558262 0,0135208
ν12*ν12 −0,0549004 0,0347382
σMDt*σMDt −0,0530247 0,0277955
σZDt*σMDZD −0,0429891 0,0269654
sigmaMDt 0,0428467 0,0141495
σMDZD*σMDZD −0,0421998 0,0287076
G13*G13 −0,0373081 0,0263084
k*k −0,0368204 0,0215034
σMDt*εC −0,0355774 0,0245434
σMDt*σZDt −0,0344273 0,0261786
k 0,0343795 0,0116436
m −0,0317261 0,0126923
E3*εC 0,0308755 0,0233089
σMDc*εC 0,0307039 0,0240288
εC*εC −0,0303422 0,0276915
σMDc*m −0,0283872 0,0232045
E1*σMDt 0,0277027 0,0264054
E3*E3 −0,0257973 0,0264745
σMDt*σMDZD 0,025198 0,0255415
E1 −0,0239148 0,013401
G13 −0,0220335 0,0122058
ν12*σMDt −0,0212226 0,027222
E1*m 0,0196765 0,024456
εC*k 0,0184676 0,0229479
σMDZD*k 0,0184197 0,0226447
sigmaMDc 0,0177553 0,0130556
k*m 0,0175188 0,0203226
sigmaZDt 0,0170921 0,0143371
E3 −0,00676466 0,0128111
nu12 −0,00312532 0,0155901

N = 156 Q2 = 0,699 Cond. no. = 13,53
DF = 121 R2 = 0,821 RSD = 0,02248
R2 adj. = 0,770
Confidence = 0,95

```
DF = 120 R2 = 0,995 RSD = 14,28
R2 adj. = 0,994
Confidence = 0,95
```